ADVANCED HEALTHCARE MATERIALS
www.advhealthmat.de

Engineering Mono-Chalcogen Nanomaterials for Omnipotent Anticancer Applications: Progress and Challenges

Chenyang Xing, Peng Yin, Zhengchun Peng, and Han Zhang**

Belonging to the chalcogen group, the elements selenium (Se) and tellurium (Te) are located in Group VI-A of the periodic table. Zero-valent nanodimensioned Se (nano-Se) and Te (nano-Te) have displayed important biomedical applications in recent years. The past two decades have witnessed an explosion in novel cancer treatment strategies using nano-Se and nano-Te as aggressive weapons against tumors. Indeed, they are both inorganic nanomedicines that suppress tumor cell proliferation, diffusion, and metastasis. Abundant synthesis strategies for rational and precise surface decoration of nano-Se and nano-Te make them significant players in resisting cancers by means of powerful multi-modal treatment methods. This review focuses on the design and engineering of nano-Se- and nano-Te-based nanodelivery systems and their precise uses in cancer treatment. The corresponding anticancer molecular mechanisms of nano-Se and nano-Te are discussed in detail. Given their different photo-induced behaviors, the presence or absence of near infrared illumination is used as a defining characteristic when describing the anticancer applications of nano-Se and nano-Te. Finally, the challenges and future prospects of nano-Se and nano-Te are summarized and highlighted.

1. Introduction

Mono-element (ME) based inorganic materials have attracted significant attention in recent years in the nano-biomedical field owing to their geometrically (0D, 1D, and 2D) and physically (optical, electrical, magnetic, mechanical, and bioactive) versatile properties.[1–15] As a pioneering example, derived from elemental carbon (C) in Group IV-A of the periodic table, graphene, the first 2D demonstration, has become vastly successful for biomedical applications, and for cancer treatments in particular.[16–21] From a geometric point of view, at least three typical morphologies of graphene with unique properties have been demonstrated, namely, 0D graphene quantum dots (GQDs), 1D carbon nanotubes,[22,23] and 2D graphene nanosheets (GNSs).[24–31] For instance, ultrasmall 0D GQDs have quantum confined dimensions, unique optical behavior, potential renal excretion and low adverse side effects.[32–35] 2D GNSs demonstrate planar construction and totally exposed surface atoms with an extremely high specific surface area and function as a rather intriguing nanoplatform or nanocarrier to load or deliver drugs.[17,36–39] Meanwhile, noble metal gold (Au)-based nanomaterials have gained significant attention, such as Au nanoparticles (NPs) and Au QDs. Investigations have shown their favorable surface plasma resonance under near infrared (NIR) irradiation to act as multifunctional photothermal therapy (PTT), photothermal dynamic therapy (PDT), photoacoustic (PA) imaging and magnetic resonance (MR) agents against cancer.[40–55] The excellent chemical and photon-mediated stability and outstanding biocompatibility of C- and Au-based nanomaterials are largely responsible for their favorable cancer treatments. Later, black phosphorous (BP), derived from elemental phosphorous (P) in Group V-A of the periodic table, followed the successful development of graphene in cancer therapy.[6,7,56–67] BP is a layered material where atom-thin layers are accumulated by van der Waals interactions, and has attracted extensive attention in the field of batteries,[68–70] photodetectors,[71] fiber lasers,[72–80] biomedicine,[81–83] and basic and applied research. It also simultaneously possesses morphologies of 0D BP quantum dots (BPQDs) and BP NPs and 2D BP nanosheets (BPNSs). It is important to note that BP has unique properties that are not found in either graphene- or Au-based nanocomposites, which may be the main reason for its popularity in nanomedicine. For instance, BP has poor chemical stability;[84,85] but this instability imbues it with excellent biodegradability for biomedical applications.[60–63,86] Besides, BP has been shown to possess a thickness-dependent energy band gap (E_g), exhibiting profitable broad-spectrum photo-induced properties.[8,64] Similar cases have been shown in other Group V-A nanocomposites including antimony (Sb)[87–89] and bismuth (Bi).[8]

Abundant evidence has proven that such ME inorganic nanomaterials have two main benefits when it comes to therapy against disease, especially cancer. The first is their role as a

Dr. C. Xing, Dr. P. Yin, Prof. Z. Peng, Prof. H. Zhang
Key Laboratory of Optoelectronic Devices and Systems of Ministry of Education
College of Physics and Optoelectronic Engineering
Shenzhen University
Shenzhen 518060, P. R. China
E-mail: zcpeng@szu.edu.cn; hzhang@szu.edu.cn

The ORCID identification number(s) for the author(s) of this article can be found under https://doi.org/10.1002/adhm.202000273

DOI: 10.1002/adhm.202000273

vehicle to carry active components, such as chemical drugs. This is because nanosized materials usually possess highly active surface areas and even surface anisotropy, allowing high loading levels. The second is their stimulus-responsive capacity in light (PTT and PDT), electricity, and magnet-induced (magnetic heating treatment) cancer treatments. These two characteristics usually go hand in hand and nanoplatforms are formed. There are several other 2D materials which can be used to construct solution-gated transistors as chemical or biological sensors, the use of which have been demonstrated in fiber lasers,[90–109] biomedicine,[110] and cancer therapy.[111] Unfortunately, these well-known nanoplatforms do not possess bioactivities themselves. In other words, they are biosafe in both normal and cancer cells. However, it is expected that inorganic nanomaterials which are bioactive and can also serve as both nanocarriers and functional entities may represent extremely promising cancer treatments.

Selenium (Se), located in Group VI-A of the periodic table, has aroused intense interest in cancer or other diseases treatment due to its distinct properties.[112–120] First, Se is a necessary trace element and nutritional component, which plays an important role in participating in activating specific enzymes in the human body. Importantly, nanosized Se (nano-Se) has been demonstrated to be an effective chemopreventive or chemotherapeutic agent for cancer treatment in view of its excellent antioxidative capacity, favorable biocompatibility, low toxicity, and excellent selectivity between normal and cancer cells. The main anticancer mechanism of nano-Se is generally accepted to be induction of cell apoptosis with overproduction of reactive oxygen species (ROS) and damage to mitochondria following activation of the corresponding signaling pathways. Obviously, the powerful self-anticancer capacity of nano-Se is absent in graphene, BP, Au and other common inorganic materials. In addition, just like BP, nano-Se is also reported to be biocompatible, with degradation products that can serve as nutritional components to be used by the host's body. From a synthesis point of view, nano-Se has a high structural plasticity because it can be obtained by a chemical route that involves the nucleation and expansion of nano-Se, during which surface decoration and modification can be done, allowing creation of many kinds of versatile nanoplatforms. Along with a self-chemotherapy mode and after decoration with polymers or biomolecules during the preparation process, nano-Se has the capacity for loading with classic small-molecule anticancer drugs, PTT agents and/or small interfering RNA (siRNA), consequently achieving a combined and multi-modal treatment comprising respectively synergistic chemotherapy, chemo-PTT, chemo-gene therapy and even radiochemotherapy against cancer. In addition, appropriate surface modifications of nano-Se can also imbue the delivery system with enhanced anticancer capacity, cancer-targeting ability, decreased multidrug resistance (MDR) and drug reversal (decreasing the side effects of the drug). It is therefore clear that nano-Se-based nanoplatforms possess great potential for cancer treatments.

Tellurium (Te) is a sister element of Se in Group VI-A. They have several similarities: first, they both have a narrow biosafe margin yet they are relatively biocompatible in nanosized forms. Second, Te- and Se-based crystals are both semiconductors with very close crystal package parameters, and nano-Te and nano-Se both possess a structural programmability, which both

Chenyang Xing is an assistant professor in the College of Physics and Optoelectronic Engineering at Shenzhen University. He received his Ph.D. in inorganic chemistry from Shanghai Institute of Applied Physics, Chinese Academy of Sciences in 2016. From 2016 to 2018, he worked as a postdoc in Professor Han Zhang's group at Shenzhen University. His research interests include design, manufacturing, and integration of 2D nanomaterials for applications in biomedical application, energy, optoelectronics, and wearable devices.

Zhengchun Peng received his Ph.D. from Georgia Institute of Technology, USA, and worked for Technology Manufacturing Group at Intel Corporation before coming back to China as part of the National Thousand Talents Program. His research interest lies in MEMS and microfluidics with a focus on high-throughput manipulation and detection of single-cell/single-molecules. At the same time, he is interested in electronic skin-based on the composite of nanofunctional materials, ion gel materials and bioelastomer materials. With advanced device design and micro–nano fabrication, he studies the electronic and photonic effects of e-skin under bending, stretching, twisting, or other external stimuli.

Han Zhang is currently distinguished professor and director of Shenzhen Engineering Laboratory of Phosphorene and Optoelectronics, Shenzhen University. He received his bachelor degree of Science in 2006 at the Department of Physics, Wuhan University, and his Ph.D. in 2010 at the School of Electrical and Electronic Engineering, Nanyang Technological University, Singapore. His research is focused on the photonic, optoelectronic and energy applications of 2D nanomaterials especially graphene, transition metal dichalcogenides (TMDCs), and black phosphorus.

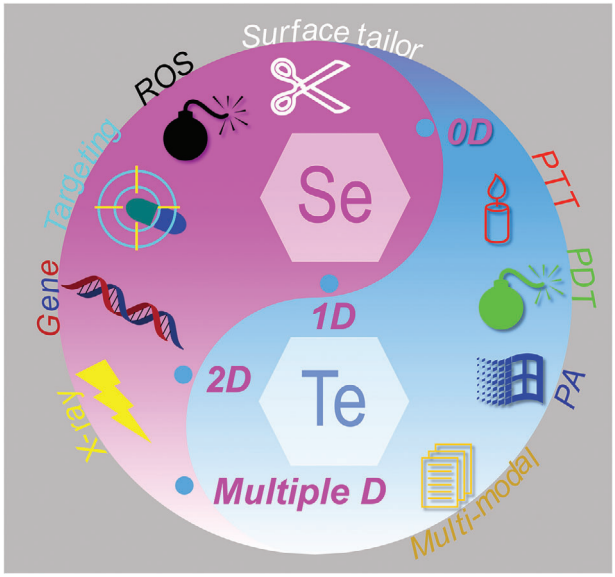

Figure 1. Overview of nano-Se and nano-Te-based cancer therapy platforms. Left: nano-Se, dual roles of nanodrug and nanocarrier. Right: nano-Te, dual roles of nanodrug and photosensitive reagent.

acquire during the transition from atoms to nanomaterials. Third, they both have self-anticancer activity. Nano-Te has thus also drawn tremendous attention in the past ten years in the field of cancer treatment. Additionally, it is interesting to find that nano-Te crystals serve as a distinctive photosensitive reagent showing excellent photo-induced properties such as photothermal and photodynamic characteristics. So, like BP, graphene oxide (GO),[19,20,121–124] and MXene,[125–132] nano-Te is also able to combat cancer by PTT and PDT treatment models under NIR light illumination. With the aid of light irradiation and its self-anticancer capacity, nano-Te represents a combined chemotherapy model to fight against cancer. In this regard, however, BP, GO, or MXene have similar combined anticancer characteristics allowing loading of additional chemical drugs.

This review summarizes the current significant progress of emerging nano-Se and nano-Te in precise cancer treatment (**Figure 1**). To start with, major types of nano-Se and nano-Te with various geometrical morphologies (0D, 1D, and 2D) and their corresponding preparation strategies are introduced, followed by respective discussions of nano-Se and nano-Te in terms of anticancer performance, including the self-anticancer molecular mechanism and combined therapeutic applications. Last, we share our insights on the challenges and future developments for this technology.

2. Strategies for Highly Stable Nano-Se and Nano-Te

Selenite (IV), seleniate (VI), tellurate (VI), and tellurite (IV) are all highly toxic.[133] Most elemental Se- and Te-based nanomaterials are commonly synthesized via a chemical approach from these high-valence anions. It is therefore clear that both nano-Se and nano-Te with high chemical stability, especially under physiological and even tumor microenvironmental conditions, are highly desirable. Like the typical preparation methodology of BP,[81] similar strategies for nano-Se and nano-Te can also be combined into "bottom-up" and "top-down" methods (**Figure 2**). According to the "bottom-up" method, the Se and Te nanomaterials can be synthesized by a redox chemical reaction. High valence Se- and Te-based salts, under the presence of reductants, can be transformed into elemental nano-Se and nano-Te. In this process, nucleation and growth dominate the physical features of the formed nano-Se and nano-Te. Extensive investigations have demonstrated that surface chemical or physical constructions of nano-Se or nano-Te are extremely significant for their therapeutic effects against cancer, and involve such activities as targeting ability, cellular uptake, biocompatibility, and stability. It is noteworthy that just a nucleation-growth process can achieve such important surface modifications for Se- and Te-based nanomaterials since newly generated Se and Te clusters have highly active specific areas, which supports opportunities for reaction with desirable functional species in the redox system. As for the "top-down" method, generally, the original sources used to fabricate nano-Se and nano-Te are bulk materials, such as Se and Te crystal powders. By chopping dimensions, Se and Te in the nanoform can be prepared (Figure 2).

2.1. Nano-Se

From a dimensional evolution (0D→1D→2D) point of view, **Figure 3** and **Table 1** display typical nano-Se structures with various surface decorations in different morphological forms. In 2012, ultrasmall 0D nano-Se dots (Figure 3a) were reported by Zheng et al.[134] Starting from gray Se powders, ultrasmall nano-Se dots with a PEG-chain decoration were fabricated by heating the Se/PEG solution at a temperature (210–220 °C) near the melting point of Se (≈217 °C). This is a typical top-down route to generate 0D nano-Se structures. Zheng and colleagues[134] developed a synthesis mechanism by which the heat-molten Se clusters from Se powders could be nanolized by reacting with the surrounding PEG chains via a possible coordination interaction of empty 4d orbitals of Se atoms with lone-pair electrons of O atoms in the PEG chains. It has also been found that the roles played by PEG in formation of 0D nano-Se are multifunctional, such as nanolizing gray Se, protecting Se from aggregation, enhancing permeability and retention effects, improving selectivity for cancer cells, and even helping to overcome drug resistance. The typical chemical route generally belongs to the bottom-up method. Elaborate choices of Se source precursors, loading templates, and even reacting "space" are advantageous for nano-Se dots. Figure 3b–d shows other reported kinds of nano-Se dots, obtained by a chemical approach. By choosing $Cu_{2-x}Se$ as a Se precursor and SiO_2 nanospheres as loading carriers,[135] Se nanodots can be deposited onto the SiO_2 nanospheres homogeneously (Figure 3b). The possible reaction mechanism can be found in the following chemical equations

$$Cu_{2-x}Se + 4(2-x)\,NH_3 + O_2 = (2-x)\left[Cu(NH_3)_4\right]^{2+} + Se^{2-} + (x/2)\,O^{2-} \quad (1)$$

Table 1. Overview of nano-Se-based nanoplatforms with mono-modal or multi-modal therapy against cancer. ADM, adriamycin; SA, sodium alginate; PEG, polyethylene glycol; MDR, multidrug resistance; 5FU, 5-fluorouracil; MUN, 11-mercapto-1-undecano; PSP, polysaccharide–protein complexes; CS, chitosan; ATP, adenosine triphosphate; FA, folic acid; BSA, bovine serum albumin; PATD, protect against toxicities of drugs; AAs, amino acids; RuPOP, ruthenium polypyridyl; siRNA, small interfering RNA; PAMAM, amine-terminated generation 5 polyamidoamine ; $G5NH_2$, dendrimers; PEI, polyethylenimine; ICG, indocyanine green; LAG, arabinogalactans; RDG, arginine-glycine-aspartic acid; HA, hyaluronic acid; PEI, polyethylenimine; PAL, *Polyporus amboinensis* lam.; HE, hawthorn fruit extract; RBCs, red blood cells; TW-80, tween-80; Cet, cetuximab; DTSSP, 3,3′-dithiobis (sulfosuccinimidyl propionate); PTR, *Pleurotus tuberregium*; PR, *Polyporus rhinoceros*; CV, *Coriolus versicolor*; GL, *Ganoderma lucidum*.

Code	D	Surface decoration	Targeting units	Functional units 1	Functional units 2	Functional units 3	Modality	Year/Ref
1	0D: 44–92 nm	Polysaccharide (*Undaria pinnatifida*)	No	No	No	No	Chemotherapy (Se)	2008[152]
2	0D: 20–70 nm	Polysaccharide (SA)	No	Adriamycin(ADM)	–	–	Chemo (ADM)-chemotherapy (Se)	2009[153]
3	0D: ≈50 nm	Sialic acid	–	–	–	–	Chemotherapy (Se)	2011[154]
4	0D: ≈50 nm	MUN	–	Cisplatin	–	–	Chemotherapy (Se);PADT	2011[155]
5	0D: <50 nm	PSP (mushroom)	–	–	–	–	Chemotherapy (Se)	2012[156]
6	0D: ≈120 nm	Chitosan (CS)	–	–	–	–	Chemotherapy (Se)	2012[157]
7	0D: 20–50 nm	Polysaccharide (Spirulina)	–	–	–	–	Chemotherapy (Se)	2012[158]
8	0D: ≈70 nm	5FU	–	5FU	–	–	Chemo (5FU)-chemotherapy (Se)	2012[139]
9	0D: ≈40 nm	ATP	–	–	–	–	Chemotherapy (Se)	2013[159]
10	0D: ≈70 nm	FA	FA	–	–	–	Chemotherapy (Se)	2013[160]
11	0D: ≈130 nm	CS	Transferrin (Tf)	DOX			Chemo (DOX)-chemotherapy (Se);PADT	2013[140]
12	0D: ≈100 nm	Trolox	–	Cisplatin	Trolox	–	Chemo (Trolox)-chemotherapy (Se);PADT	2013[161]
13	0D: ≈20 nm	BSA	–	Irinotecan	–	–	Chemo (Irinotecan)-chemotherapy (Se);PADT	2014[162]
14	0D: ≈120 nm	AAs	–	–	–	–	Chemotherapy (Se)	2014[163]
15	0D: ≈100 nm	L/D-Arginine	L/D-Arginine for chirality	siRNA	Ruthenium (II) complex		Gene (siRNA)-chemotherapy (Se); MDR	2015[164]
16	0D: ≈89 nm	Polysaccharide(*Dictyophora Indusiata*)	–	–	–	–	Chemotherapy (Se)	2015[165]
17	0D: ≈80 nm	G5.NH2	–	Cisplatin DDP	siRNA	–	Gene (siRNA)-chemotherapy (Se); MDR	2015[166]
18	0D: ≈89 nm	CS;PluronicF-127	FA	RuPOP	–	–	Chemo (RuPOP)-chemotherapy (Se);PADT	2015[167]
19	0D: ≈280 nm	Glucose	–	–	–	–	Chemotherapy (Se)	2016[168]
20	0D: 40–50 nm	PEG	–	Crocin	–	–	SynergisticChemotherapy (Se+crocin)	2016[169]

(*Continued*)

Table 1. Continued.

Code	D	Surface decoration	Targeting units	Functional units 1	Functional units 2	Functional units 3	Modality	Year/Ref
21	0D: 80–90 nm	PEI	–	siRNA	–	–	Gene (siRNA)-chemotherapy (Se);	2016[170]
22	0D: <5 nm	@porous SiO_2	–	DOX	–	–	SynergisticChemotherapy (Se+DOX)	2016[135]
23	0D: <5 nm	BSA	–	–	–	–	Chemotherapy (Se)	2016[136]
24	0D: <120 nm	@Gold nanorod	CS-RGD CS-ACPP	–	–	–	Radiochemotherapy(X-ray)	2017[171]
25	0D: ≈ 53 nm	Curcumin	–	Curcumin	–	–	SynergisticChemotherapy (Se+Curcumin)	2017[172]
26	0D: ≈ 127 nm	Liposome	–	DOX	–	–	SynergisticChemotherapy (Se+DOX)	2017[173]
27	0D: ≈ 100 nm	FA-CS-PEG	FA	Baicalin	–	–	SynergisticChemotherapy (Se+Baicalin)	2017[174]
28	0D: ≈ 180 nm	CS	Tf	–	–	–	Radiochemotherapy(^{125}I)	2017[175]
29	0D: ≈ 50 nm	FA-CS	FA	DOX			SynergisticChemotherapy (Se+DOX)	2017[176]
30	0D: ≈ 110 nm	CS	RC-12 peptide; PG-6 peptide	DOX	ICG		Chemo(DOX and Se)-PTT	2018[177]
31	0D: <5 nm	@porous SiO2	–	ICG	DOX	–	Chemo(DOX and Se)-PTT	2018[178]
32	0D: ≈120 nm	PAMAM	RGD	DOX	siRNA	–	Gene (siRNA)-chemotherapy (Se+DOX);	2018[179]
33	1D: 400 × 100 nm^2	FA	FA				Chemotherapy (Se) (enhanced)	2018[180]
34	0D: 70–180 nm^2	HA-PEI	HA	siRNA	–	–	Gene (siRNA)-chemotherapy (Se);	2018[181]
35	0D: <5 nm	@porous SiO2	FA	DOX	CuS		Chemo(DOX and Se)-PTT	2018[182]
36	0D: ≈100 nm	Polysaccharides (PAL)	PAL	–	–	–	Chemotherapy (Se) BBB	2018[183]
37	0D: ≈100 nm	Natural polymer (HE)	HE	–	–	–	Chemotherapy (Se)	2018[184]
38	0D: ≈200 nm	PEG-RBC	–	Bevacizumab	–	–	Radiotherapy+antiangiogenesis (X-ray)	2018[185]
39	0D: ≈ 90–160 nm	Polysaccharide (LAG)	–	–	–	–	Chemotherapy (Se)	2019[186]
40	0D: ≈ 60 nm	Polysaccharide (laminarin)	–	–	–	–	Chemotherapy (Se)	2019[187]
41	0D: ≈ 70 nm	TW-80	Cet	5FU	PAMAM-DTSSP	Gadolinium (MRI)	Chemotherapy (Se)	2019[188]
42	0D: ≈ 10–20 nm	Polysaccharide (PTR/PR/CV/GL)	–	–	–	–	Chemotherapy (Se)	2019[189]

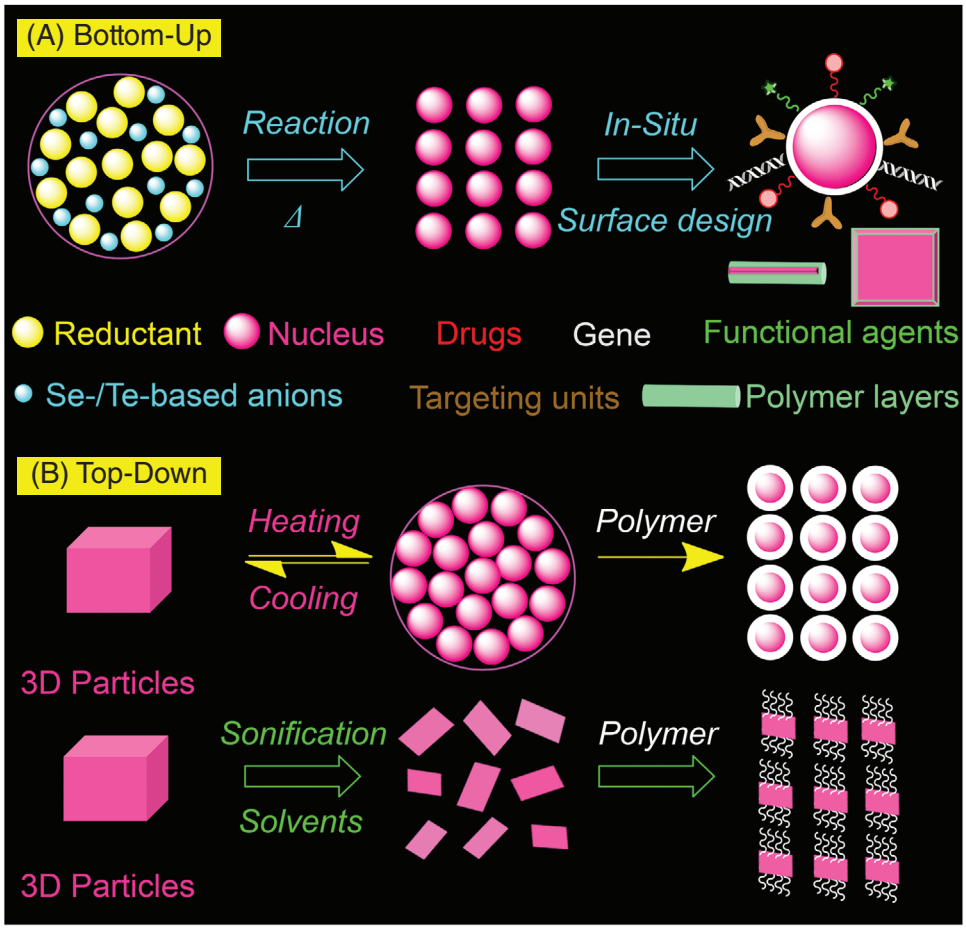

Figure 2. Schematic illustration of the synthesis methods of functional nano-Se or nano-Te: a) bottom-up synthesis (chemical route) and b) top-down fabrication (physical route).

$$Se^{2-} + O_2 = Se \downarrow + (1/2)\, O^{2-} \quad (2)$$

It is believed that newly produced Se atoms and/or clusters are highly reactive with high energy active surfaces, inevitably aggregating with each other without any surface decorations or anchors. In this study, SiO_2 nanospheres served as anchors to support active sites for loading of Se atoms or clusters. Consequently, the newly formed Se atoms or clusters on the surface of the SiO_2 nanospheres could not grow further, let alone aggregate, generating morphologies with ultrasmall dimensions. Similarly, when the Se source and loading scaffold were adopted to Na_2SeSO_3 and bovine serum albumin (BSA) respectively, both amorphous and crystalline nano-Se dots could be obtained, as shown in Figure 3c,d, respectively.[136] It was noted that in this study, elemental Se was produced under acid conditions, even in the presence of BSA by the following equation

$$Na_2SeSO_3 + 2HCl = 2NaCl + Se \downarrow + SO_2 \uparrow + H_2O \quad (3)$$

In another study, Gao et al.[137] reported hollow sphere nano-Se by using a specific template-interface reaction, as shown in Figure 3e. In their study, protein A (Pr) was used as a template, which can form a protein–water interface to support loading sites for the generated Se atoms that were reduced from sodium selenite (Na_2SeO_3) and mercaptoethanol (CH_3CH_2SH). The intermediate $Se(SCH_2CH_3)_2$ could have weak interactions with Pr via NH, CN, C = O, and COO^- groups. Such an interaction caused the formed Se nucleates to be localized at the Pr–water interface, finally forming amorphous hollow nano-Se.

According to the literature, apart from 0D nano-Se with either ultrasmall or hollow morphologies, the most reported 0D nano-Se are compact and have dimensions of several tens of nanometers (Figure 3f–h). Such kinds of nano-Se are usually prepared by a chemical route. For instance, Zhang's group[138] reported nano-Se with an average particle size of 24 nm and a modification of natural hyperbranched polysaccharide (HBP) (Figure 3f). The obtained HBP-capped nano-Se were extremely stable and water-dispersible. The HBP macromolecules played important roles in stabilizing and protecting nano-Se. Zhang's study is actually a classic and simple model, namely, polymer + nano-Se. Furthermore, Liu et al.[139] reported nano-Se with a modification of 5-fluorouracil (5FU) (Figure 3g), a common anticancer chemotherapy drug. It was found that 5FU can also help to improve nano-Se by enhancing stability and homogeneity. A possible chemical bonding of Se–O and Se–N between Se and 5FU could be responsible for this improvement. It is obvious that this is a

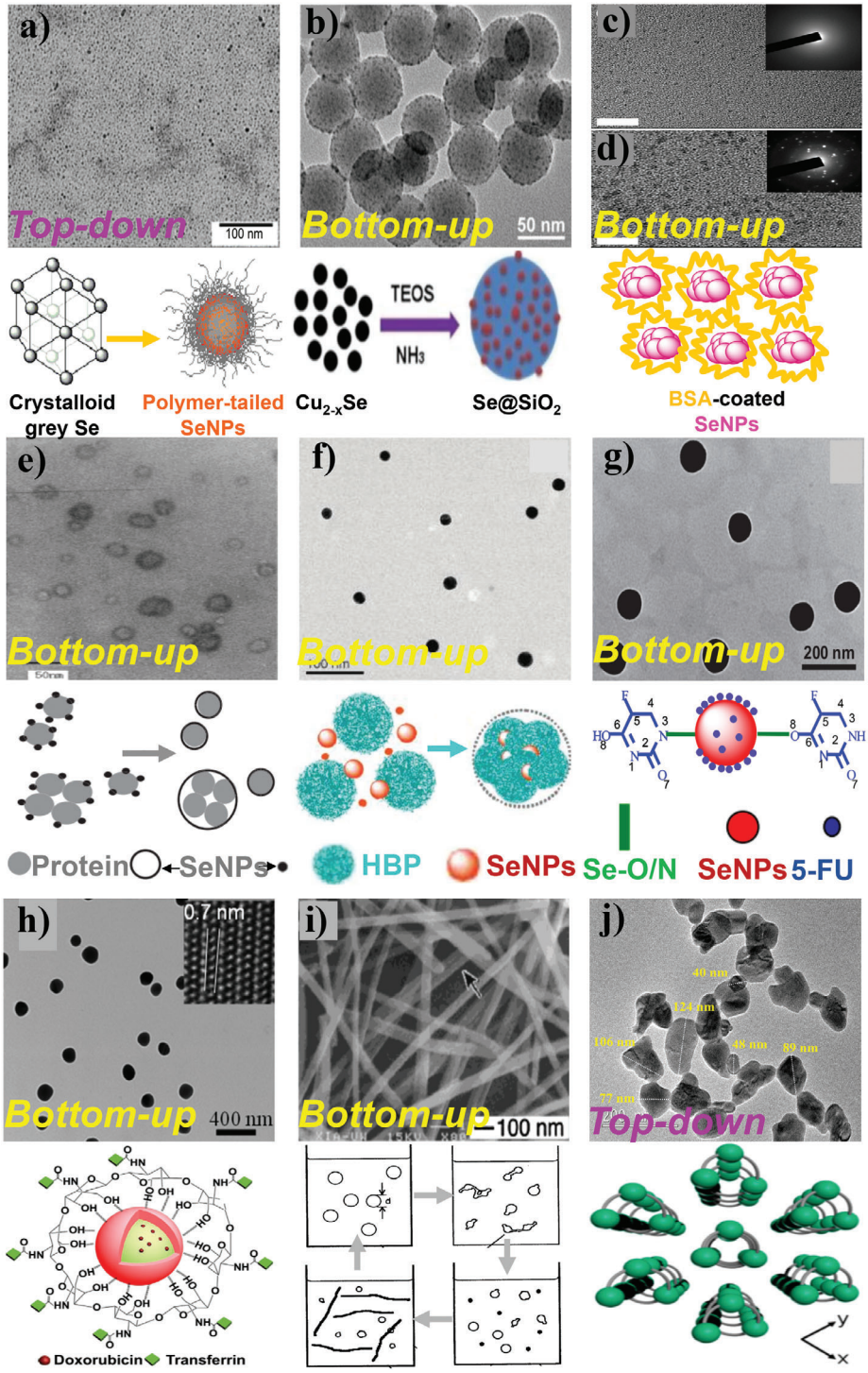

Figure 3. Nano-Se structures with 0D, 1D, and 2D geometrical morphologies. a) 0D PEG-chain-tailed Se nanodots. Reproduced with permission.[134] Copyright 2012, Dove Medical Press Ltd. b) 0D Se nanodots anchored within porous SiO_2 nanoparticles. Reproduced with permission.[135] Copyright 2016, The Royal Society of Chemistry. 0D bovine serum albumin chain-decorated Se nanodots with amorphous c) and crystalline d) characteristics. Reproduced with permission.[136] Copyright 2016, Nature Publishing Group. e) 0D porous Se nanostructures. Reproduced with permission.[137] Copyright 2002, Wiley-VCH. f) 0D hyperbranched polysaccharide (HBP) (polymer) surface-modified compact Se nanoparticles (polymer + nano-Se). Reproduced with permission.[138] Copyright 2010, American Chemical Society. g) 0D drug 5-Flurouracil (5FU) surface-modified Se nanoparticles (drug + nano-Se). Reproduced with permission.[139] Copyright 2012, American Chemical Society. h) 0D Se nanoparticle with surface decorations of chitosan (CS) polymer chains and a drug and cancer-targeting units (Tf) (polymer + drug +nano-Se). Reproduced with permission.[140] Copyright 2013, Elsevier Ltd. i) 1D Se nanowires. Reproduced with permission.[141] Copyright 2000, American Chemical Society. j) 2D Se nanosheets with small-dimensioned structures. Reproduced with permission.[142] Copyright 2017, American Chemical Society (chain-like structures). Reproduced with permission.[143] Copyright 2017, Wiley-VCH (2D morphologies).

model of drug + nano-Se. This drug would not only exert its capacity against cancer but also serves as a capping agent, as seen with polymer. In addition, the third commonly reported nano-Se is based on the above two models, that is, polymer + drug + nano-Se. For example, Huang et al.[140] reported a versatile nano-Se-based nanoplatform, as shown in Figure 3h. The roughly 120 nm sized nano-Se were composed of positively charged chitosan (CS) chains, negatively charged chemical drug doxorubicin (DOX) and a targeting ligand, transferrin (Tf). The polymer modifications of CS for nano-Se were multiple, including stabilizing Se nanoparticles, physical interactions with DOX and chemical bonding with Tf molecules. It is accepted that nano-Se first decorated with polymers or bio-macromolecules can be rationally designed with multifunctionality.

In addition to 0D nano-Se structures, 1D and 2D nano-Se have also been demonstrated. For 1D nano-Se, Gates et al.[141] previously reported uniform Se nanowires with a diameter of 10 to 30 nm and a length of several micrometers (Figure 3i). It is interesting that the obtained 1D Se nanowires underwent a solid–solution–solid transformation, unlike other direct-synthesis processes. The 0D spherical Se nanoparticles with amorphous nature (a-Se) were prepared first. After the cooling of this a-Se solution, small amounts of nanocrystallites of trigonal Se (t-Se) precipitated out in the solution, serving as seeds for t-Se nanowires. The long-term aging of the above solution in the dark resulted in 1D nanowires. As for 2D nano-Se, Xing et al.[143] first reported small-sized 2D Se nanosheets by applying a simple liquid-phase exfoliation (LPE) method (Figure 3j), belonging to the top-down group of methods. Although the Se crystal is not a typically layered material, it is characterized as a chain-like structure.[142] The bonding difference between Se–Se chemical bonds in intrachain and chain–chain van der Waals' forces gives rise to an anisotropy, which can be used to fabricate 2D Se nanosheets by the LPE method. Compared with 0D and 1D nanostructures, 2D morphologies can provide improved specific surface areas, implying the potential of loading diverse chemical species. It is therefore rational that surface modification of these 2D nano-Se has potential applications in biomedicine.

The above preparation of nano-Se in different morphological forms can be chosen for a specific purpose in practical application. Elaborate surface modification, by polymer, drug, targeting ligand or other functional inorganic materials such as photothermal agents, contrast agent, and even DNA or RNA, can support opportunities to achieve multi-model combined therapy against cancer. It is therefore possible that by modifying the above three models with a certain purpose, nano-Se-based nanoplatforms can be expanded for promising biomedical applications. Unfortunately, it should be noted that the above 0D hollow Se spheres[137] and 2D Se nanosheets[142,143] have not yet been demonstrated in biomedical applications, but may yet generate interesting results in view of their unique geometric morphologies.

2.2. Nano-Te

Like the previously described nano-Se, there have also been three kinds of nano-Te demonstrated for use in cancer therapy in the literature, namely, 0D-, 1D- and 2D-based nanostructures. It is interesting that despite their anticancer capacity nano-Te-based nanoplatforms usually exert their anticancer capacity under the assistance of NIR light illumination, namely, light-mediated cancer therapy. This is mainly ascribed to the excellent photothermal, photodynamic, photoacoustic properties of nano-Te in view of its good semiconductor characteristics.

Figure 4 shows typical nano-Te in its 0D, 1D, and 2D forms. Yang et al. reported a chemical synthesis route for 0D Te-nanodots (0D nano-Te) in 2017.[144] In their study, just like the nano-Se that can form 0D morphology if given a suitable template scaffold, human serum albumin (HSA) was adopted not only as a surface decoration agent but a nanocage to restrict the further growth of Te crystals. It was proposed that the Te source TeO_3^{2-} ions had specific interactions with HSA protein molecules. When the elemental Te atoms occurred (nucleation) by a reduction reaction, they may anchor onto the HSA scaffold, which hindered further growth of Te and generated ultrasmall-sized crystal Te-nanodots (Figure 4a). The prepared Te-nanodots were about 6–8 nm in diameters (Figure 4b) and highly crystalline (Figure 4c). Generally, this type of 0D nano-Te nanostructure had a core–shell structure in which Te nanocrystals served as an inner core and HSA nanocage as an outer shell. One of the advantages of 0D nano-Te is based on their long-term retention at the tumor site and post-treatment renal excretion due to their ultrasmall dimensions. Another investigation into 0D Te-nanodots (≈3 nm) was reported by Wen et al. in 2019.[147] They chose mesoporous silica nanoparticles (MSNs) as the anchor for loading Te-nanodots. MSNs have tunable and stable pore structures, and high specific surface area, and they can also support a size-limited reaction space to assist with the formation of ultrasmall Te-nanodots. As a result, water-dispersible carboxyl-functionalized MSNs served as scaffolds to bear Te-nanodots under reduction conditions. Owing to their chain-like structures, Te-based nanostructures tended to form 1D morphologies (such as nanowires) with lengths of tens of micrometers, which doubtlessly are too large for biomedical applications. Considering the difficulty in obtaining 1D Te nanostructures of short length, Yu et al.[145] fabricated 1D Te-nanoneedles with reduced length (<500 nm) by meticulous control of experimental conditions, such as temperature, reaction time and the choice of polymers for surface modification. As shown in Figure 4d, NH_2OH and reduced glutathione (GSH) were both adopted as reductants, and polyvinylpyrrolidone (PVP) polymer was chosen to protect the Te crystals. Prolonging the reaction time could further elongate Te-nanoneedles in lateral length (Figure 4e,f). The obtained Te-nanoneedles were found to have a high yield of up to 86% and have a high crystallinity (Figure 4g).Compared with 0D- and 1D-Te nanostructures, 2D Te may possess considerably enhanced specific surface areas, thus supporting a very large probability of successful loading of diverse and specific-purpose species. Ye's group reported PVP-mediated 2D Te-nanosheets by using a common hydrothermal reaction.[148,149] However, they were several micrometers in lateral dimension, despite their ultrathin features. He and colleagues also previously reported 2D Te nanoplates.[150] Yet, similarly, the Te nanoplates were also too large and their preparation conditions were so harsh that a high yield was not readily achieved. Recently, Xie et al.[151] first reported small-sized 2D Te nanosheets by using a simple LPE method. Following this pioneering work, Lin et al.[146] reported GSH-modified 2D Te nanosheets by using a similar LPE strategy, generating 2D Te

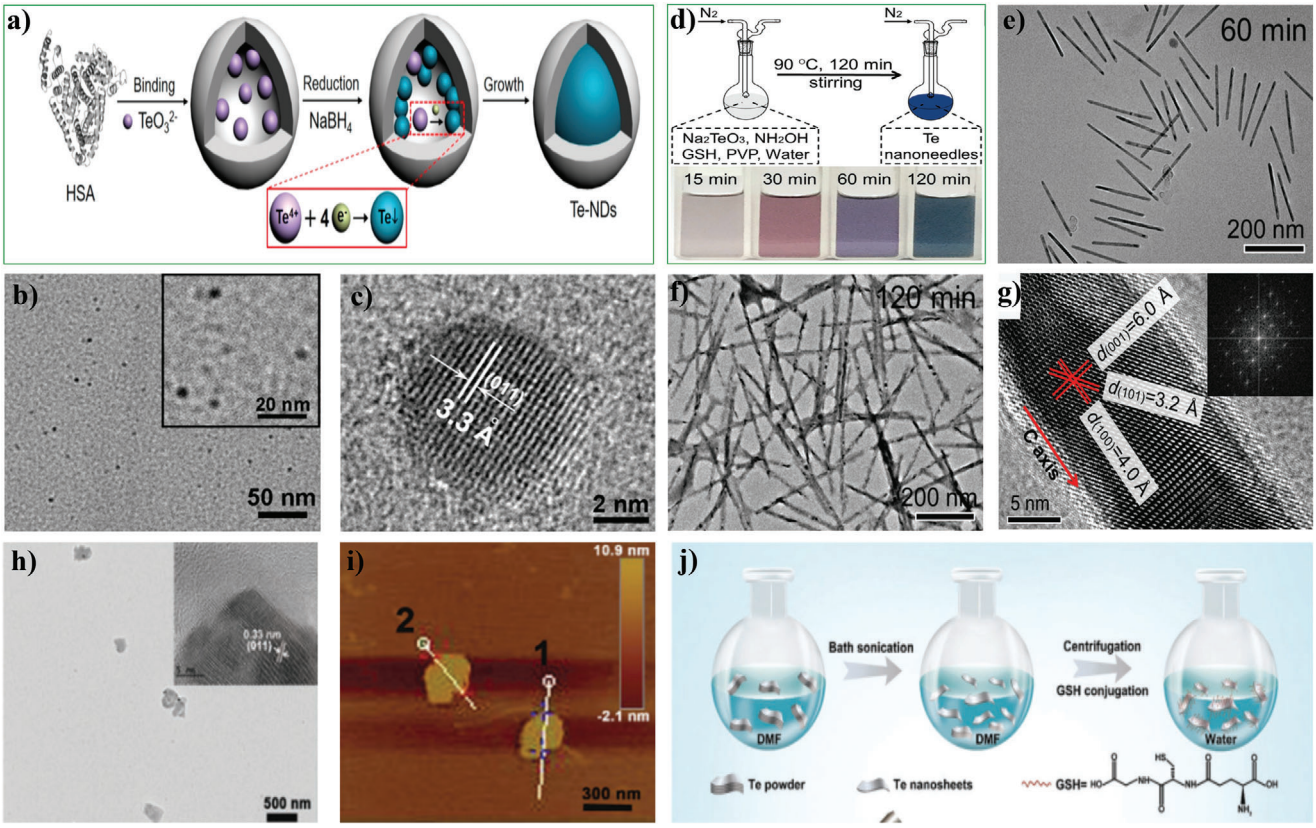

Figure 4. Nano-Te structures with 0D, 1D, and 2D geometrical morphologies: 0D Te nanodots (Te NDs) a–c); Reproduced with permission.[144] Copyright 2017, American Chemical Society. 1D Te nanoneedles d–g); Reproduced with permission.[145] Copyright 2018, Wiley-VCH. 2D Te nanosheets h–j). Reproduced with permission.[146] Copyright 2018, The Royal Society of Chemistry. a) Schematic of synthesis of Te NDs with the aid of BSA-based nanocages. b) Transmission electron microscope (TEM) image of Te-NDs. c) High-resolution (HR) TEM image of single Te-ND showing clear crystalline lattice fringe. d) Schematic of synthesis of short Te nanoneedles in the presence of glutathione (GSH) and polyvinylpyrrolidone (PVP). e,f) Reaction time-dependent morphologies of Te nanoneedles. g) HR-TEM image of single Te nanoneedle, with fast-Fourier transform pattern (inset). h) TEM and HR-TEM images of Te nanosheets. i) Atomic force microscopy of Te nanosheets showing their thickness. j) Typical liquid-phase exfoliation to fabricate Te nanosheets with surface modification by GSH.

nanosheets with a lateral dimension of about 300 nm (Figure 4h) and a thickness of about 10 nm (Figure 4i). The LPE-generated Te nanosheets were post-treated by mixing Te nanosheets with GSH polymer solution (Figure 4j). The GSH-polymer surface decoration not only improved the stability of Te nanosheets but also their biocompatibility. It should be noted that Te-based inorganic salts are highly toxic and that naked Te crystals are not chemically stable, degrading into Te-containing high valent ions, such as TeO_3^{2-} and TeO_4^{2-}. Thus, it can be speculated that the toxicity of Te nanostructures may arise from their degradation products. Therefore, improving the stability of Te-based nanostructures can enhance their biocompatibility.

3. Nano-Se for Combating Cancer

It is believed that naked inorganic elemental nano-Se is usually met with several obstacles impeding its further biomedical application. For unmodified nano-Se, the absence of effective groups and/or modification layers can cause unstable storage, uncertain toxicity, unfavorable cellular uptake, poor selectivity between cancer and normal cells and even inadequate anticancer efficiency. Fortunately, most synthesized nano-Se originates from high valence Se-based sources (i.e., Se-based precursors), and desirable chemical or physical functionalization can be achieved during the process of nucleation and growth of nano-Se. As for modified nano-Se, further functionalization can be realized for versatile applications. In this section, we introduce the anticancer activity of modified nano-Se, including its self-anticancer capacity, molecular mechanism, and its combined models against cancer.

3.1. Self-Anticancer Capacity of Nano-Se

Most inorganic nanomaterials are currently being used as nanocarriers in biomedical applications. For instance, graphene and BP are excellent nanocarriers due to their high specific surface areas and superficial wrinkled structures, respectively. In addition, GO has also played an important role in acting as a nanocarrier because of its abundant polar functional groups including hydroxy (–OH), carboxyl (–COOH) and epoxy groups on the surface. It should be noted that these famous examples of nanocarriers are usually used solely as nanocarriers and that they are not bioactive in cancer treatments. In other words, most

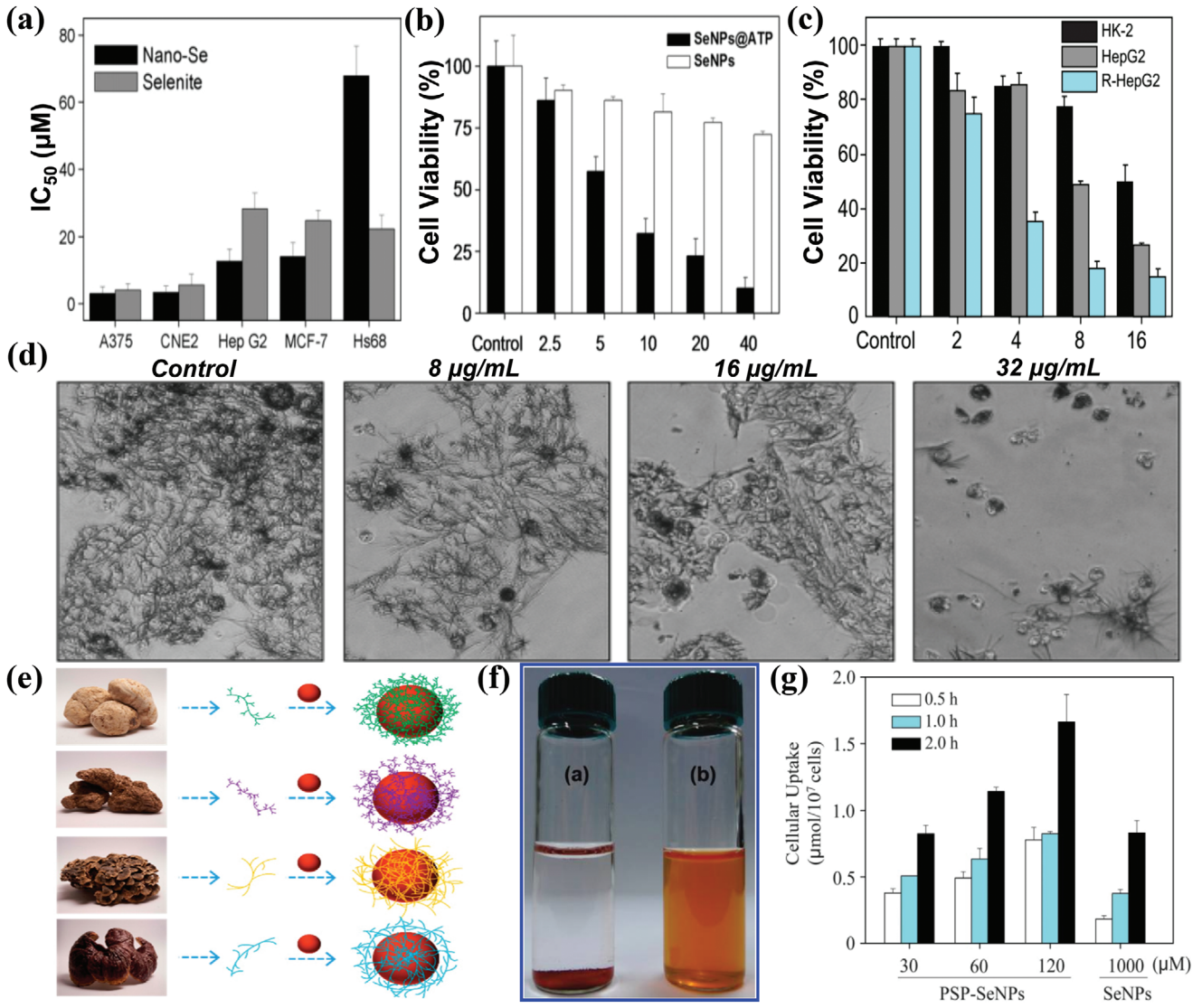

Figure 5. Self-anticancer activity of nano-Se with appropriate surface modifications by various polymers. a) Anticancer effects of polysaccharide (from *U. pinnatifida*)-modified nano-Se and selenite on the various human cancer cell lines (A375, CNE2, Hep G2, and MCF-7) and normal cells (Hs68 human fibroblasts). Reproduced with permission.[152] Copyright 2008, Elsevier B.V. b) Concentration (μM)-dependent cell viability of HepG2 cells for adenosine triphosphate (ATP) surface-functionalized nano-Se (i.e., SeNPs@ATP) and unfunctionalized Se nanoparticles (SeNPs). Reproduced with permission.[159] Copyright 2013, Elsevier Inc. c) Concentration (μg mL^{-1})-dependent cell viability of PEG-nanolized ultrasmall nano-Se (PEG-SeNPs) towards human tumor HepG2 cells, drug-resistant HepG2 cells (R-HepG2) and normal cells (human kidneyHK-2 cells), respectively. Reproduced with permission.[134] Copyright 2012, Dove Medical Press Ltd. d) Morphology of R-HepG2 cells treated with PEG-SeNPs for 72 h at various concentrations. Reproduced with permission.[134] Copyright 2012, Dove Medical Press Ltd. e) Polysaccharides, extracted from natural resources, used to decorate nano-Se: *Pleurotus tuber regium*, *Polyporus rhinoceros*, *Coriolus versicolor,* and *Ganoderma lucidum* (from top to bottom). Reproduced with permission.[189] Copyright 2019, American Chemical Society. f) Photographs of 48 h storage of aqueous nano-Se without (left, a) and with (right, b) modification with hyperbranched polysaccharide (HBP). Reproduced with permission.[138] Copyright 2010, American Chemical Society. g) Time-dependent cellular uptake of nano-Se with and without modifications of polysaccharide–protein complexes (PSP). Reproduced with permission.[156] Copyright 2018, The Royal Society of Chemistry.

inorganic nanocarriers are biocompatible with both normal and tumor cells. Things are different when it comes to nano-Se that possesses the dual capacities of being a nanocarrier and of being bioactive to combat cancer.

Selenite, the main precursor of nano-Se, is well known to be highly toxic, reflecting growth inhibition of a broad spectrum of human cancer cell lines including A375, CNE2, Hep G2, and MCF-7,[152] as shown in **Figure 5**a. However, selenite is also cytotoxic for noncancerous Hs68 human fibroblasts, which means it cannot differentiate cancerous cells from normal, and thus lacks specificity between the two. Interestingly, Se in the nano-sized form, namely, nano-Se, with a surface modification by using *Undaria pinnatifida*-extracted polysaccharide, has a similar and even higher anticancer activity than that of selenite shown in Figure 5a, with much lower IC_{50} values for the cancer cell lines mentioned above.[152] Furthermore, for normal cells, nano-Se can

induce a significantly enhanced IC_{50} value, compared with selenite, suggesting a considerably improved biocompatibility. In other words, Se in nanosized form can not only largely decrease its toxicity for normal cells but holds improved anticancer capacity. It should also be noted that nanosized Se is superior to ionic selenite to act as a nanocarrier due to its superhigh surface areas. In this regards, nano-Se itself has indeed dual roles in combating cancer. It has also been found that the anticancer activity of nano-Se can be further enhanced by surface modifications. As shown in Figure 5b, adenosine triphosphate (ATP) surface-functionalized selenium nanoparticles (SeNPs@ATP) can cause an obvious decrease in cell viability for HepG2 cells in a dose-dependent manner, relative to naked Se nanoparticles.[159] Additionally, nano-Se also has positive effects on MDR. For instance, PEG-nanolized ultrasmall nano-Se (PEG-SeNPs) demonstrates both cell growth inhibition of human tumor HepG2 cells and drug-resistant HepG2 cells (R-HepG2), the latter of which is much more sensitive to PEG-SeNPs (Figure 5c).[134] The PEG-SeNP-treated R-HepG2 cells exhibited decreased cell numbers, loss of cell-to-cell contact, cell shrinkage and formation of apoptotic bodies in a concentration-dependent manner (Figure 5d). In 2019, Zeng et al.[189] systematically investigated polysaccharides extracted from natural resources to modify nano-Se with the aim of determining the relationship between surface decoration and tumor selectivity (Figure 5e). It is accepted that several significant benefits can be obtained by means of decorating nano-Se. First, the surface modification can stabilize the nano-Se with significantly increased stability and homogeneity (Figure 5f).[138] This is because the surface layers of nano-Se can support steric hindrance to hinder further growth of nano-Se. Water-soluble and biosafe polymers have important roles in tailoring the dimensions and stability of nano-Se. Second, the surface modification has the capacity to enhance cellular uptake due to improved cancer-targeting features (Figure 5g).[156] It is well accepted that lectin–carbohydrate, ligand–receptor, and antibody–antigen are key means by which the cancer targeting of nanomaterials is realized and enhanced.[158] Investigations have shown that tumor cells and malignant tissues contain lectins on their surfaces. So, carbohydrate moieties can be used to target lectins for tumor-targeting therapy. In this regard, the surface modification induced improvement of cellular uptake of nano-Se may be ascribed to these targeting mechanisms. Third, surface modification of nano-Se can significantly enhance the anticancer activity. Based on the above two discussions, it is undoubted that the anticancer activity of nano-Se can be significantly enhanced not only by improving the biocompatibility for normal cells but by heightening the cytotoxicity for tumor cells.

3.2. Molecular Anticancer Mechanism

The anticancer mechanisms of nano-Se are of great significance and are also vital to guide the construction of nano-Se-based nanomedicine platforms with multi-modal activities against cancer. According to the literature, from an intracellular toxicity point of view, tumors may undergo a series of biological events before induction of apoptosis by nano-Se, such as the initial uptake of nano-Se, overproduction of ROS and the corresponding altered apoptosis-associated proteins under specific apoptotic signaling pathways, and changes to the relevant organelles. Conversely, considering the important roles played by the cell membrane in cellular biological activities, to assess and investigate the biomechanical properties of nano-Se-exposed tumor cells can also contribute to understanding the mechanism of nano-Se against cancer. **Figures 6** and **7** depict the two main anticancer mechanisms of nano-Se.

As reported by Yu et al.[190] in Figure 6, nano-Se with a curcumin (Cur)-loading and a folate-chitosan (FAC)-surface-decoration could enter MCF-7 tumor cells by endocytosis. Results can be concluded as follows: 1) nano-Se entered tumor cells by typical endocytosis. By employing specific fluorescence probes (Lyso Tracker Red for lysosomes and DAPI for cell nuclei of tumor cells), the colocalization of nano-Se and lysosomes in MCF-7 cells could be observed and the intensity was found to increase in a time-dependent manner (Figure 6a). Subsequently, nano-Se escaped from the lysosome (3 h) was released into the cytosol and distributed within the cell (6 h) (Figure 6a). 2) Induction of apoptosis was considered to be mainly responsible for nano-Se-induced inhibition of cancer cell proliferation. This was reflected by the considerably increased Sub-G1 populations in a nano-Se dose-dependent manner and the lack of significant changes in cell cycle distribution (G0/G1, S, and G2/M). In addition, DNA fragmentation and nuclear condensation further confirmed apoptosis. 3) ROS overproduction (Figure 6b). Western blot analysis suggested that JNK and ERK in the MAPK family and PI3K/Akt pathways were associated with ROS-induced apoptosis. For instance, nano-Se exhibited significant effects on the expression of phosphorylated Akt in a dose-dependent manner (Figure 6c). Furthermore, it also triggered the phosphorylation of JNK and downregulated phosphorylation of ERK (Figure 6c). In addition, nano-Se showed a significant inhibitory effect on the expression of phosphorylated NF-κB that binds with DNA in the nucleus. It is believed that overproduction of DNA leads to accumulation of DNA oxidative products. Results showed that exposure of MCF-7 tumor cells to nano-Se resulted in enhancement of phosphorylated ATM, phosphorylated Brca1 and phosphorylated p53 (Figure 6c), suggesting the involvement of the ROS-activated p53 signaling pathway induced by nano-Se. 4) Depletion of mitochondrial membrane potential ($\Delta\psi_m$) (Figure 6d). The mitochondria-mediated apoptotic pathway contributes to nano-Se-induced apoptosis. Nano-Se significantly increased the expression of the pro-apoptosis proteins Bad and Bax in a dose-dependent manner (Figure 6e). It can be concluded that exposure of tumor cells to nano-Se can induce DNA damage, Akt and ERK dephosphorylation and result in activation of the p53 pathway and inhibition of the NF-κB pathway, which in turn trigger mitochondrial dysfunction to amplify the apoptotic signals (Figure 6f). According to Liao et al.[165] caspase activation was also involved in nano-Se-induced HepG2 cancer cell apoptosis. As shown in Figure 6g, polysaccharide (DP1)- (extracted from *Dictyophora indusiata*) modified nano-Se (DP1-SeNPs) caused significant increases in caspase-3 (effector), and caspase-8 and caspase-9 (initiators) in a dose-dependent manner. In view of caspases-8 and -9 acting as initiators of the death receptor-mediated and mitochondria-mediated apoptotic pathways, respectively, both the death receptor-mediated and mitochondria-mediated apoptotic pathways are involved in the DP1-SeNP-induced apoptosis. In addition, the expression level of Fas-associated death domain

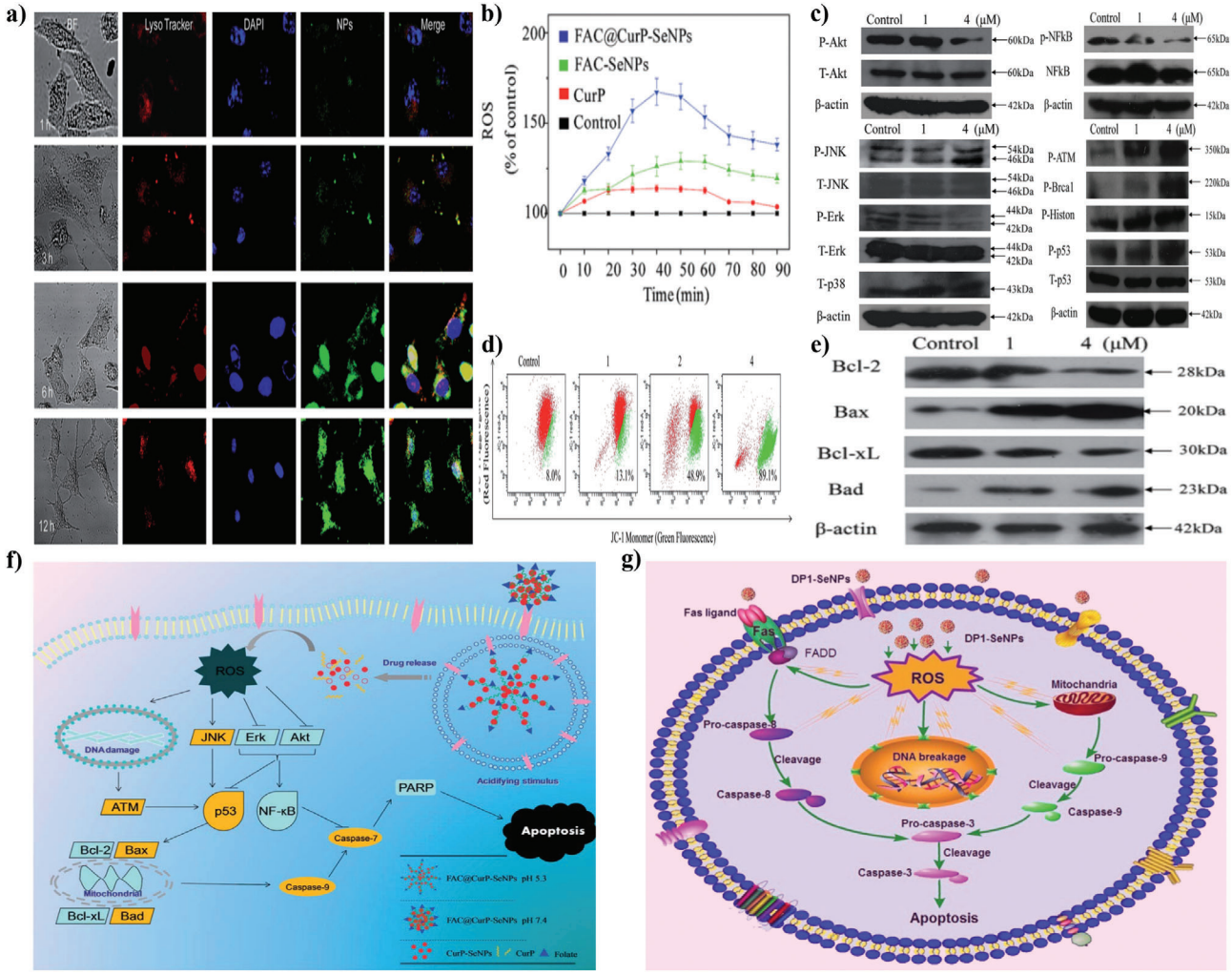

Figure 6. Anticancer molecular mechanism of nano-Se, from a cellular toxicity point of view. a) Confocal microscope images of FAC@CurP–SeNP-treated MCF-7 cells, showing the intracellular fate (localization) of nano-Se (FAC@CurP–SeNPs). DAPI (cell nucleus; blue) and lyso tracker (lysosome; red) were used as fluorescent probes. Reproduced with permission.[190] Copyright 2014, The Royal Society of Chemistry. b) Changes in reactive oxygen species (ROS) levels within MCF-7 cells following different treatments (FAC@CurP-SeNPs, FAC-SeNPs, and CurP). c) Effects of FAC@CurP–SeNPs on phosphorylation status and expression levels of Akt, ERK, p38MAPK, JNK, NF-κB and DNA damage-associated proteins. d) Depletion of mitochondrial membrane potential in MCF-7 cells induced by FAC@CurP–SeNPs. e) Effects of FAC@CurP–SeNPs on the expression levels of Bad, Bcl-xl, Bax, Bcl-2 in MCF-7 cells. f) Proposed signaling pathways of apoptosis induced by FAC@CurP–SeNPs in MCF-7 cells. Reproduced with permission.[190] Copyright 2014, The Royal Society of Chemistry. g) Proposed signaling pathways of HepG2 cell apoptosis induced by polysaccharide extracted from the fungus *Dictyophora indusiata* (DP1) modified nano-Se (DP1–SeNPs). Reproduced with permission.[165] Copyright 2015, Nature Publishing Group.

protein (FADD) in HepG2 cells was also significantly enhanced as DP1-SeNP concentration increased, indicating that activation of FADD is also involved inDP1-SeNP-induced apoptosis.

The cell membrane has been considered to be a vital target in typical chemotherapy, and it is therefore logical that its biomechanical properties could also influence the death of cancer cells induced by nano-Se. In this regard, atomic force microscopy (AFM) can be applied as a useful detection tool to assess the surface changes of nano-Se-exposed cancer cells. Luo et al.[191] first employed a Si_3N_4 tip in AFM measurement to scan the surface of treated HeLa cells in 2012. It was found that HeLa cells without exposure to nano-Se exhibited clear and intact morphology with typical invasive cell characteristics, such as dense filopodia and lamellipodia in the terminal area (Figure 7a). The smooth cell surface gave a low surface roughness value of 74.8 nN (Figure 7a). However, when treated with 10×10^{-6} M nano-Se, the HeLa cells became considerably shrunken in morphology and highly increased in surface roughness at 227.8 nN (Figure 7b). Later, in 2013, Pi et al.[192] systematically investigated the adhesion force and Young's modulus of MCF-7 cells before and after treatment with nano-Se. As shown in Figure 7c, the adhesion force maps of MCF-7 cells showed a transformation from high (control group, red patterns) to low adhesion force intensity (nano-Se treated group, blue patterns), suggesting a decrease in adhesion force of tumor cells after exposure to nano-Se. Furthermore, the average adhesion force values significantly decreased from 2131 ± 664 pN for the control group to 1834 ± 844 pN for the nano-Se-exposed group. This means that the adhesion

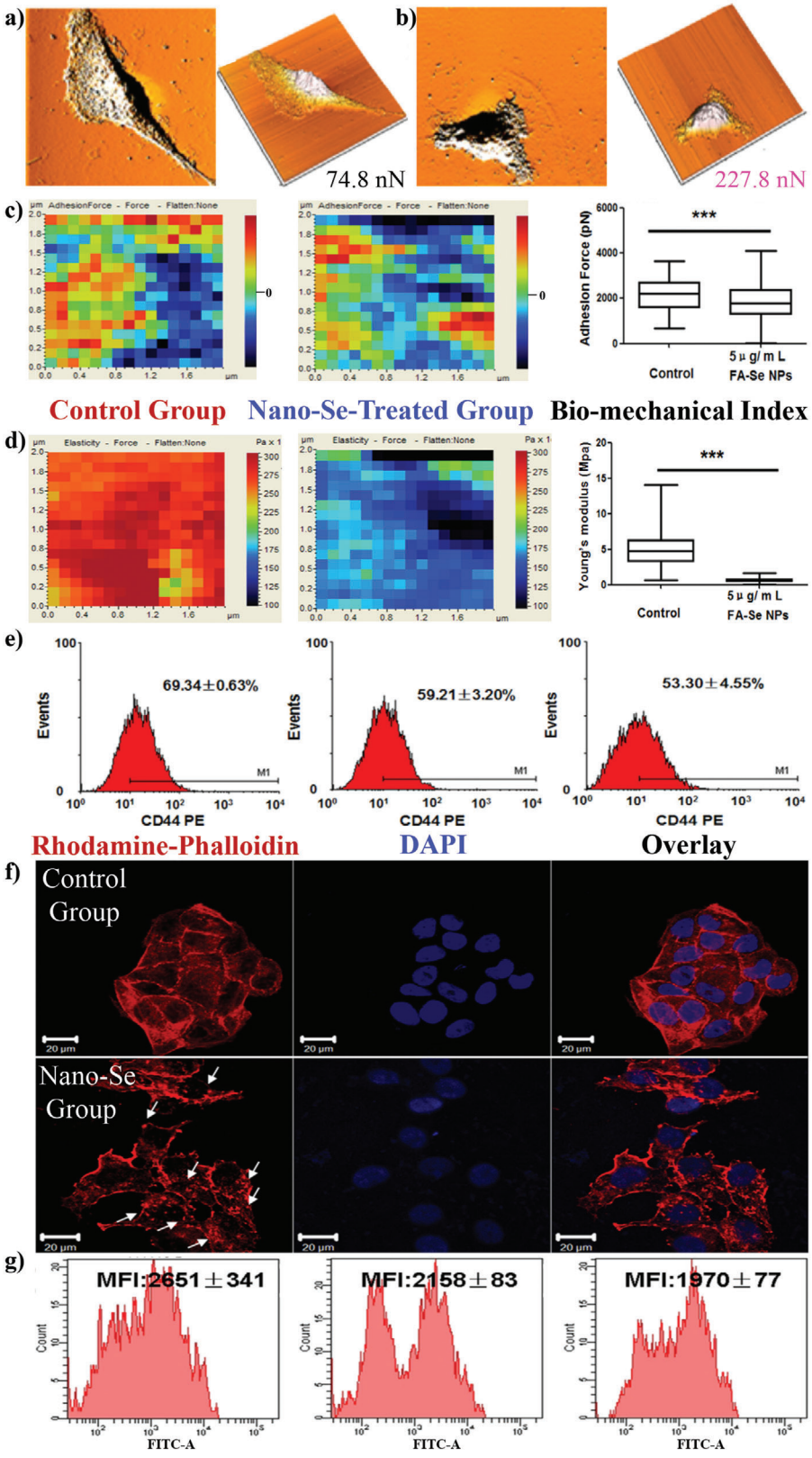

capacity between the MCF-7 cell membrane and the AFM tip was weakened, implying that the lesion of MCF-7 cell induced by nano-Se. Additionally, Young's modulus map of tumor cells in Figure 7d also showed a similar decreased tendency, from 5.05 ± 2.43 MPa for the control group to 0.69 ± 0.31 MPa for the nano-Se-treated group, a sign of MCF-7 cells becoming soft after treatment with nano-Se. The adhesion force between the MCF-7 cell membrane and AFM tips is in fact the interaction of chemical molecules on the membrane with inorganic tips. In view of this consideration, CD44, a native trans-membrane protein participating in the regulation of diverse and significant cellular processes, was detected before and after nano-Se treatment. The results showed a dose-dependent decrease of CD44 expression (Figure 7e), suggesting a downregulatory relationship between CD44 and nano-Se, contributing to the apoptosis of MCF-4 cells. The cell cytoskeleton, mainly composed of actin and tubulin proteins, plays important roles in shaping a cell and providing mechanical rigidity, thus any alterations may be responsible for the observed changes of Young's modulus of cells. At this point, to assess the changes of F-actin, which is regarded as the major cytoskeletal component of cells, both in terms of morphology and concentration in MCF-7 cells, could lead to a better understanding of the underlying mechanism behind the alteration of Young's modulus in MCF-7 cells. As shown in Figure 7f, normal MCF-7 cells, stained by rhodamine-labeled phalloidin, displayed a homogeneous cytoplasmic distribution of F-actin without observation of any changes in stress fiber morphology. After exposure to nano-Se for 24 h, the F-actin in MCF-7 cells became aggregated and formed dot-like structures (white arrows, Figure 7f). In addition, the amount of intracellular F-actin in MCF-7 cells was also found to be considerably decreased, as shown in Figure 7g. Consequently, it can be concluded that the decrease in Young's modulus of nano-Se-treated MCF-7 cells can be attributed to the disturbed or depolymerized structure and the decreased amount of F-actin in MCF-7 cells. Losing the biomechanical properties of the cell membrane and the cytoskeleton in MCF-7 cells gradually resulted in the apoptosis of these cells. Therefore, investigating the biomechanical properties of tumor cells before and after nano-Se treatment can further help to understand the molecular mechanism of apoptosis induced by nano-Se, without intracellular toxicity assessment.

3.3. Multimodal Cancer Treatment by Nano-Se

3.3.1. Chemo-Gene Therapy

It is generally accepted that chemotherapeutic drugs used nowadays exert a complicated impact on cancer, in that they exhibit moderate therapeutic efficacy but generate some serious side effects and may cause induction of MDR. The overexpression of P-glycoprotein (P-gp), a member of the ATP-binding cassette superfamily, is considered to be a mechanism of MDR. It is therefore logical that downregulating the expression of P-gp or inhibiting P-gp function may be a good strategy to overcome MDR in cancer therapy. In this regard, gene therapy, which has the potential to overcome MDR by silencing the expression of P-gp through RNA interference thus restoring intracellular drug levels and inducing cell apoptosis, combined with chemotherapy, has been considered an effective strategy to overcome MDR. For example, in 2015, Zheng et al.[166] reported nano-Se-based chemo-gene therapy to combat cancer (**Figure 8**a). In their investigation, generation five polyamidoamine (PAMAM) dendrimer (G5) was applied to decorate nano-Se, which not only stabilized the nano-Se particles but acted as nanocarriers to simultaneously carry cisplatin (*cis*-diamminedichloroplatinum-(II), DDP) and siRNA via the interior void space (Figure 8a). The G5 modified nano-Se was found to have high transfection efficiency and low toxicity. The effects of nano-Se-based complexes on the expression of MDR proteins in tumor cells are shown in Figure 8b. P-gp was overexpressed in A549/DDP cells to a high level. DDP and naked siRNA could not downregulate P-gp levels, indicating obvious MDR in A549/DDP cells. However, treatment withG5-siRNA, G5@Se-siRNA and, especially, G5@Se-DDP-siRNA showed an obvious downregulation of P-gp levels, suggesting the validity of combined chemo-gene therapy against MDR in cancer therapy. Additionally, compared with naked DDP, the DDP loaded within G5@Se was found to be less reactive with GSH (Figure 8c) and MT (Figure 8d), which were both involved in detoxification. This indicated that by being loaded onto G5@Se complexes, the intracellular efficacy of DDP was enhanced and sensitivity to this drug was restored in A549/DDP cells. Similarly, Huang et al.[179] also reported a synergistic precise cancer chemo-gene therapy by means of multifunctional nano-Se-based platforms (Figure 8e). In this demonstration, they fabricated an intriguing core–shell nanoplatform, where the core was DOX-loaded Se nanoparticles and the shell was c-myc siRNA delivered by PAMAM-arginine-glycine-aspartic acid (RGD) peptide. The use of the RGD peptide targeting ligand can achieve cancer-target delivery. The results showed that owing to the PAMAM-RGD decoration, the nano-Se platform had a higher transport ratio across the blood brain barrier of about 40.3% compared with DOX-loaded SeNPs (13.2%) and PAMAM-decorated DOX-SeNPs (17.6%), which suggested an efficient penetrating effect of the nano-Se platform. Furthermore, because of this excellent penetrating capacity, the PAMAM-RGD-decorated DOX-Se exhibited high permeability, as shown in Figure 8f. It was observed that DOX-loaded SeNPs displayed weak fluorescence intensity and the PAMAM-modified DOX-SeNPs showed slightly increased fluorescence intensity. In sharp contrast, PAMAM-RGD-decorated DOX-Se showed the

Figure 7. Anticancer molecular mechanism of nano-Se, from a biochemical point of view. Atomic force microscopy (AFM) images of a) Hela cells and b) nano-Se treated Hela cells at a 10×10^{-6} M concentration. Reproduced with permission.[191] Copyright 2012, Elsevier B.V. c) Typical adhesion force maps of MCF-7 cells in the absence (control group) and presence (nano-Se-treated group) of nano-Se treatment, and the adhesion force comparison between the two groups. d) Typical Young's modulus maps of MCF-7 cells in the absence (control group) and presence (nano-Se-treated group) of nano-Se treatment, and the Young's modulus results comparison between the two groups. e) The effects of nano-Se concentration on expression of CD44 molecules in MCF-7 cells (nano-Se concentrations were 0, 2.5 and 5 μg mL^{-1}, from left to right). f) Fluorescence staining of F-actin structures in MCF-7 cells with (nano-Se group) and without (control group) nano-Se treatment. g) The effects of nano-Se concentration on F-actin in MCF-7 cells (nano-Se concentrations were 0, 2.5 and 5 μg mL^{-1}, from left to right). Reproduced with permission.[192] Copyright 2013, Elsevier Ltd.

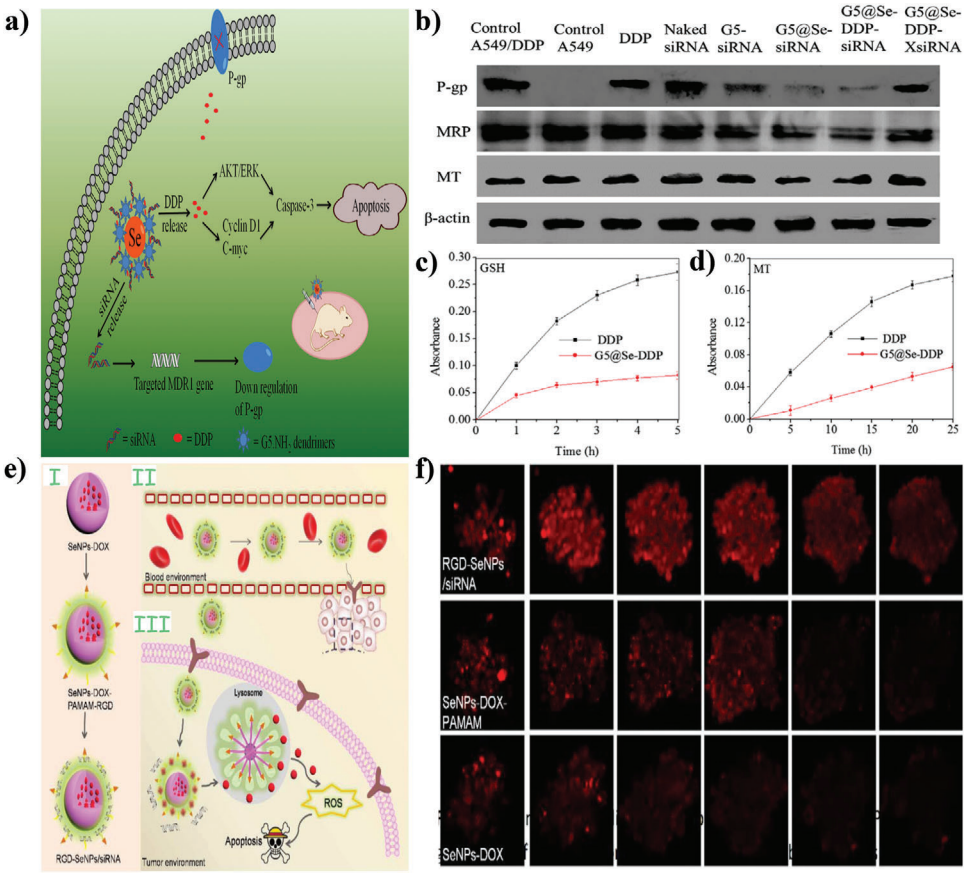

Figure 8. Synergistic chemo-gene therapy with nano-Se. a) Nano-Se-based dual-delivery system: nano-Se (nanocarrier as well as nanoagent), amine-terminated generation five polyamidoamine (PAMAM) ($G5.NH_2$) dendrimers (surface modifier), short interfering (si) RNA and cisplatin (*cis*)-diamminedichloroplatinum-(II) (DDP; drugs). b) Expression of P-gp, MRP and MT in A549/DDP cells after 24 h incubation with various nanoplatforms indicated, including DDP, naked siRNA, G5-siRNA, G5@Se-siRNA and G5@Se-DDP-siRNA, respectively. c) Time-dependent absorbance of glutathione (GSH) and d) MT after reactions with DDP and G5@Se-DDP at 37 °C, pH 7.4. Reproduced with permission.[166] Copyright 2015, Elsevier Ltd. e) Nano-Se-based cancer-targeted and pH-responsive multifunctional nanoplatforms made of nano-Se (nanocarrier as well as nanoagent), PAMAM dendrimers, doxorubicin (DOX) and siRNA (drugs), and arginine-glycine-aspartic acid (RGD) peptide (targeting ligand). f) Confocal laser scanning microscope images of tumor spheroids treated with RGD-SeNP/siRNA, SeNP-DOX-PAMAM, and SeNP-DOX, showing differing permeabilities. Reproduced with permission.[179] Copyright 2018, The Royal Society of Chemistry.

best penetrating ability with a 30 μm depth in tumor spheroids. This excellent permeability and anticancer activity is likely to be responsible for the significant tumor growth inhibition ability of such a PAMAM-RGD-decorated DOX-Se platform. The improved permeability of this nanosystem can be ascribed to the specific recognition of RGD and the protonation effect of PAMAM under the acidic microenvironment of the tumor.

3.3.2. Chemo-Radiotherapy

Radiotherapy is one of the most frequently used cancer therapy methods utilizing irradiation from a variety of radiation sources. Unfortunately, its therapeutic efficacy is often limited by the radiation resistance of hypoxic tumor cells. A high radiation dose may cause damage near the focal location and other side effects. Developing effective radiosensitizers to increase the local radiotherapy treatment efficacy under a relatively low and safe radiation dose has been demonstrated to be of great significance. Nano-Se has shown effectiveness as an intriguing nanosensitizer to improve the therapeutic effect of cancer treatment by combining its chemotherapeutic role with enhancement of radiotherapy. Chan et al.[175] reported a nano-Se platform-based synergetic chemo-radiotherapy against cancer in 2017 (**Figure 9**a). In their investigation, nano-Se particles were conjugated by CS and Tf to improve biocompatibility, stability in the physiological environment and selectivity between tumor and normal cells. The Iodine-125 (^{125}I) seed was applied to emit γ-ray via attenuation of the I atom to achieve radiotherapy. The clear elemental Se-rich and Fe-rich images in Figure 9b,c suggested successful decoration with CS and Tf on the surface of the nano-Se. A comprehensive comparison of single chemotherapy and chemo-radiotherapy under X-ray and ^{125}I seed irradiation was made to evaluate the synergistic therapeutic efficacy. It was found that Tf-decorated nano-Se (Tf@SeNPs) alone caused only a slight increase in the Sub-G1 value, indicating insufficient inhibition of tumor cell proliferation. This situation was clearly improved under X-ray irradiation but with a high radiation dose of 6 Gy. However, the

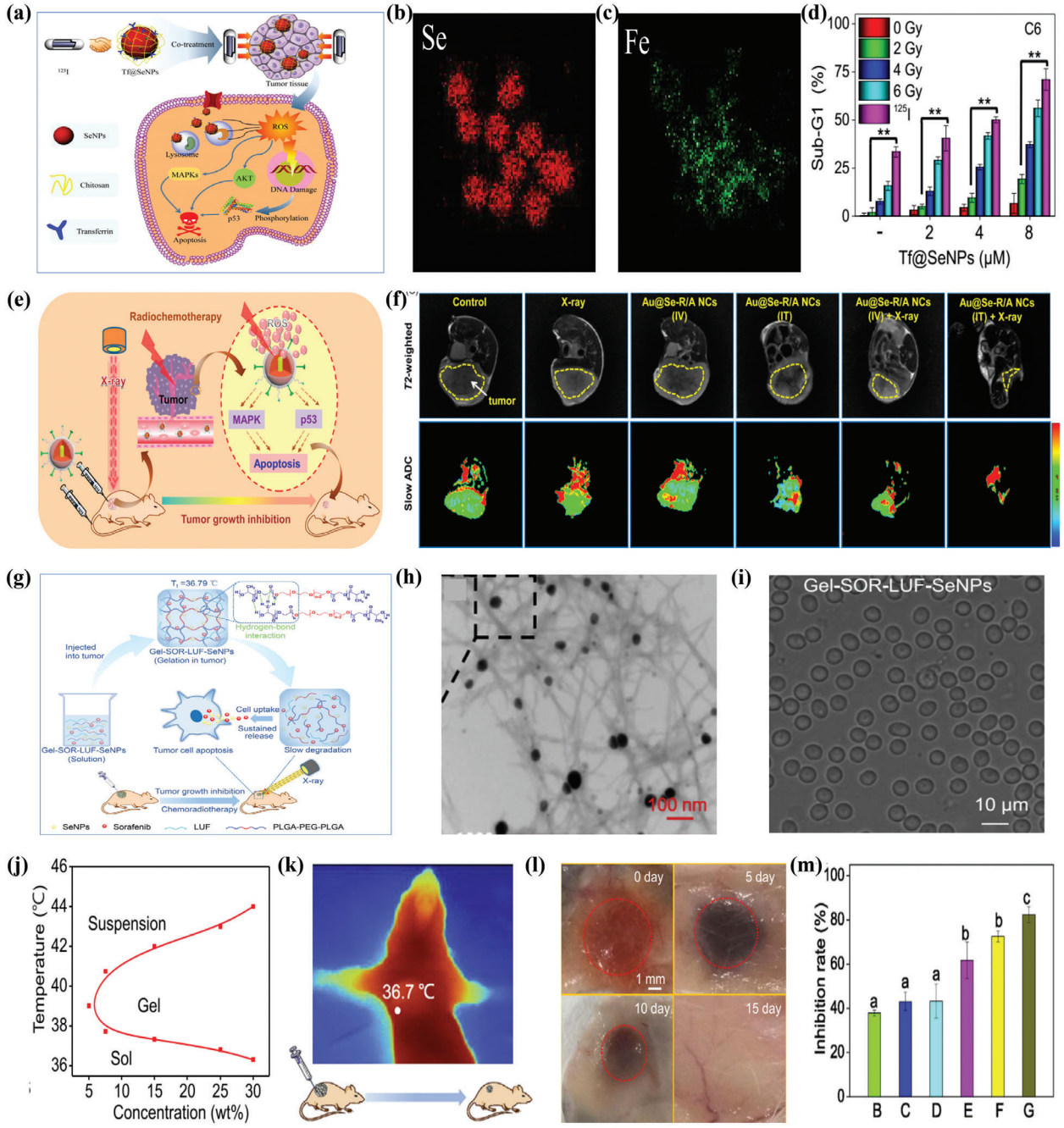

Figure 9. Synergistic chemo-radiotherapy with nano-Se. a) Schematic showing mechanisms of cancer-targeted nano-Se-based nanoplatform: chitosan (CS)- and transferrin (Tf)-modified nano-Se (nanocarrier, nanoagent and radiation sensitizer) and ^{125}I seeds (γ-ray irradiation); HAADF-STEM images of Tf@SeNPs showing b) Se- and c) Fe-element images. d) Quantization of Sub-G1 phase in C6 cells treated with Tf@SeNPs (0, 2×10^{-6}, 4×10^{-6}, and 8×10^{-6} M) with or without X-ray irradiation (2, 4, and 6 Gy) and ^{125}I seeds (2 Gy), respectively. Reproduced with permission.[175] Copyright 2017, Wiley-VCH. e) Nano-Se@nano-Au rod-based novel nanoplatforms: nano-Se (shell), nano-Au rod (core), with CS-modified arginine-glycine-aspartic acid (RGD) and CS-modified ACPP (tumor-cell-targeting peptides) and X-ray irradiation. f) T_2-weighted magnetic resonance (MR) images show apparent diffusion coefficient of A375 tumor-bearing mice at day 21 following differing treatments. The tumor sites were in the back region and indicated by dashed lines. Reproduced with permission.[171] Copyright 2017, American Chemical Society. g) Nano-Se-based injectable thermosensitive hydrogels: nano-Se (nanoagent and radiation sensitizer), sorafenib (SOR; drug), lipiodol (LUF) and poly (D,L-lactic acid-*co*-glycolic acid)-*b*-poly (ethylene glycol)-*b*-poly (D,L-lactic acid-*co*-glycolic acid) (PLGA-PEG-PLGA; thermosensitive polymer matrix). h) 3D network structure with embedding of CS-modified nano-Se and SOR. i) Hemocompatibility of nano-Se-based hydrogels. j) Phase diagram of PLGA-PEG-PLGA triblock copolymer. k) Photothermal image of HepG2 tumor-bearing mice with a temperature close to the sol–gel transition temperature of PLGA-PEG-PLGA. l) In vivo degradation behaviors of nano-Se-based hydrogels at the indicated time point after subcutaneous injection (scale bar, 1 mm). m) Tumor inhibition rate of various nanoplatforms, including B) X-ray (2 Gy), C) CS-SeNPs, D) SOR, E)SOR-SeNPs-based gel, F) SOR-SeNPs-LUF-based gel, and G) SOR-SeNPs-LUF-based gel with a 2Gy-X-ray. Reproduced with permission.[193] Copyright 2019, Elsevier Inc.

Sub-G1 value was significantly enhanced by Tf@SeNPs with ^{125}I seed irradiation at a low dose of 2 Gy at the same Se concentration. These results suggested that nano-Se can serve as an interesting radiosensitizer to improve anticancer activity. The same year, Chang et al.[171] designed nano-Se- and nano-Au-based core–shell nanocomposites (NCs), and investigated systematically the radio-chemotherapeutic effect of cancer treatment under X-ray irradiation (Figure 9e). Au nanorods were first prepared, followed by coating or growth of the Se shell, generating Au@Se NCs. To improve biocompatibility and cancer-targeting ability of the Au@Se NCs, CS-modified RGD (R) and ACPP (A) peptides were employed to decorate, thus producing Au@Se-R/A NCs. With the modification of cancer-targeting ligands, the nano-Se complex platform showed increased anticancer activity and cellular uptake. It was also found that the co-treatment of Au@Se-R/A NCs and X-ray irradiation caused considerably increased ROS levels relative to single therapies. The synergistic therapeutic efficacy of chemo-radiotherapy of Au@Se-R/A NCs may due to the additional ROS generation by Au atoms that absorb X-rays to produce photons and then ROS species. In addition, T_2-weighted MR images in Figure 9f have further proven this synergistic therapeutic efficacy. For instance, for Au@Se-R/A NCs with X-rays, larger slow apparent diffusion coefficient signals were observed, indicating significant inhibition of tumor cells (Figure 9f).

In 2019, Zheng et al.[193] reported an injectable thermosensitive nanocomposite based on nano-Se for localized synergistic chemo-radiotherapy (Figure 9g). It is noted that a second cancer drug of sorafenib (SOR), excepting for nano-Se, was employed. Owing to the serious side effects of SOR via oral administration and its poor water solubility, the authors embedded the SOR, together with CS-modified nano-Se, into a thermosensitive nanosystem based on a triblock copolymer of poly (D,L-lactic acid-*co*-glycolic acid)-*b*-poly (ethylene glycol) -*b*-poly (D,L-lactic acid-*co*-glycolic acid) (PLGA-PEG-PLGA) (Figure 9g). The obtained SOR-SeNP-loaded PLGA-PEG-PLGA nanocomposite showed a 3D network structure (Figure 9h) and excellent hemocompatibility (Figure 9i). It was found that such a nanoplatform possessed a polymer-concentration-dependent sol–gel transition temperature (Figure 9j).The temperature of tumor-bearing nude mice was detected to be 36.7 °C (Figure 9k), which was close to the sol–gel transition temperature, suggesting the SOR–SeNP-loaded PLGA–PEG–PLGA nanocomposite could form a gel in mice, which supported local therapy with sustained drug release to improve therapeutic efficacy. Furthermore, the intriguing nano-Se-based platform also exhibited favorable degradation behavior in vivo (Figure 9l). Taken together, under X-ray treatment, such a nano-Se-based platform showed desirable anticancer activity relative to other single therapy models (Figure 9m).

3.3.3. Chemo-Photothermal Therapy

Chemical synthesis approaches have been demonstrated to be versatile for building multifunctional nano-Se-based platforms. It is accepted that newly generated Se atoms reduced from high valence Se-based ions possess superhigh surface energy and that they readily aggregate with each other. However, uncontrollable size and morphology as well as subsequent instability of naked nano-Se largely contributes to its rare use in clinical applications. Considerable evidence has suggested that surface modifications by polymers (macromolecules structure), drugs (small molecules), and inorganic materials (solid templates) can produce simultaneously stable and functional nano-Se complexes. As a result, the final nano-Se system has in fact many functional groups or polymer chains, which can further graft other functional chemical species. Nano-Se has played a unique role in tumor chemotherapy, regardless of chemical drug loading. When thermal agents are loaded onto the nano-Se platforms, a combination of chemotherapy (from nano-Se with or without other drugs) and PTT under NIR light irradiation can be achieved. For instance, in 2018, Fang et al.[177] fabricated nano-Se-constructed cancer-targeting nanoplatforms for synergistic PTT and chemotherapy against cancer. The nano-Se nanoplatforms were designed as follows (**Figure 10**a). First, the introduction of DOX and CS-bonded targeting ligands (RC-12 and PG-6 peptides) during the formation of nano-Se gave rise to nano-Se structures with CS polymer chains, amino acid groups and acylamino groups of peptides. Second, due to these functional tails, indocyanine green (ICG), serving as a PTT agent, was further introduced into the above nano-Se system in the presence of PVP, finally forming SeNP-DOX-ICG-RP nanocomposites (Figure 10a). This nano-Se-based multifunctional complex showed excellent photothermal properties (Figure 10b) with high photothermal conversion as well as stability. This means the disadvantages of ICG including severe photobleaching may be overcome by integration with nano-Se. Importantly, the nano-Se platform was found to effectively inhibit the migration of HepG2 tumor cells, as shown in Figure 10c. Without NIR irradiation, the nano-Se complex showed only a marginal inhibitory effect on migration of tumor cells. Interestingly, the migration-inhibiting effect of the nano-Se complex was largely improved under NIR irradiation in a nano-Se-loading-dependent manner (Figure 10c,d). In addition, it also was observed that SeNP-DOX-ICG-RP nanocomposites could cause additional ROS production following NIR stimulation (Figure 10e). Owing to their excellent photothermal properties, inhibition of tumor cell migration and induction of ROS, the nano-Se platform has been found to effectively inhibit tumor proliferation when combined with NIR treatment at much lower IC_{50} values than control groups without NIR irradiation (Figure 10f,g).

Chemical drugs, such as DOX, usually demonstrate a lack of tumor-specific targeting ability and thus kill both normal and tumor cells, causing severe side effects. So, not only do they have a narrow therapeutic window but possess high toxicity to normal cells. Precise solutions to these drawbacks of chemical drugs have been much debated. Fortunately, nano-Se has been demonstrated to effectively reverse the side effects of cancer treatment drugs. In this regard, integrating nano-Se with DOX raises the possibility of achieving the double goal of chemotherapeutic efficacy against cancer with limited drug-induced side effects. When PTT agents were loaded onto DOX-loaded nano-Se, a synergistic therapeutic effect of chemotherapy and PTT was obtained. It is interesting that when the nano-Se system was porous, the DOX-release could be light-controlled with NIR irradiation because the NIR-induced heat accelerated the release rate of DOX. As a result, at the tumor site, the effective concentration of DOX was largely enhanced by laser illumination, generating an enhanced therapeutic effect. In 2018, Wang et al.[182] constructed a targeted nano-Se-based chemotherapy-PTT combined delivery system. They

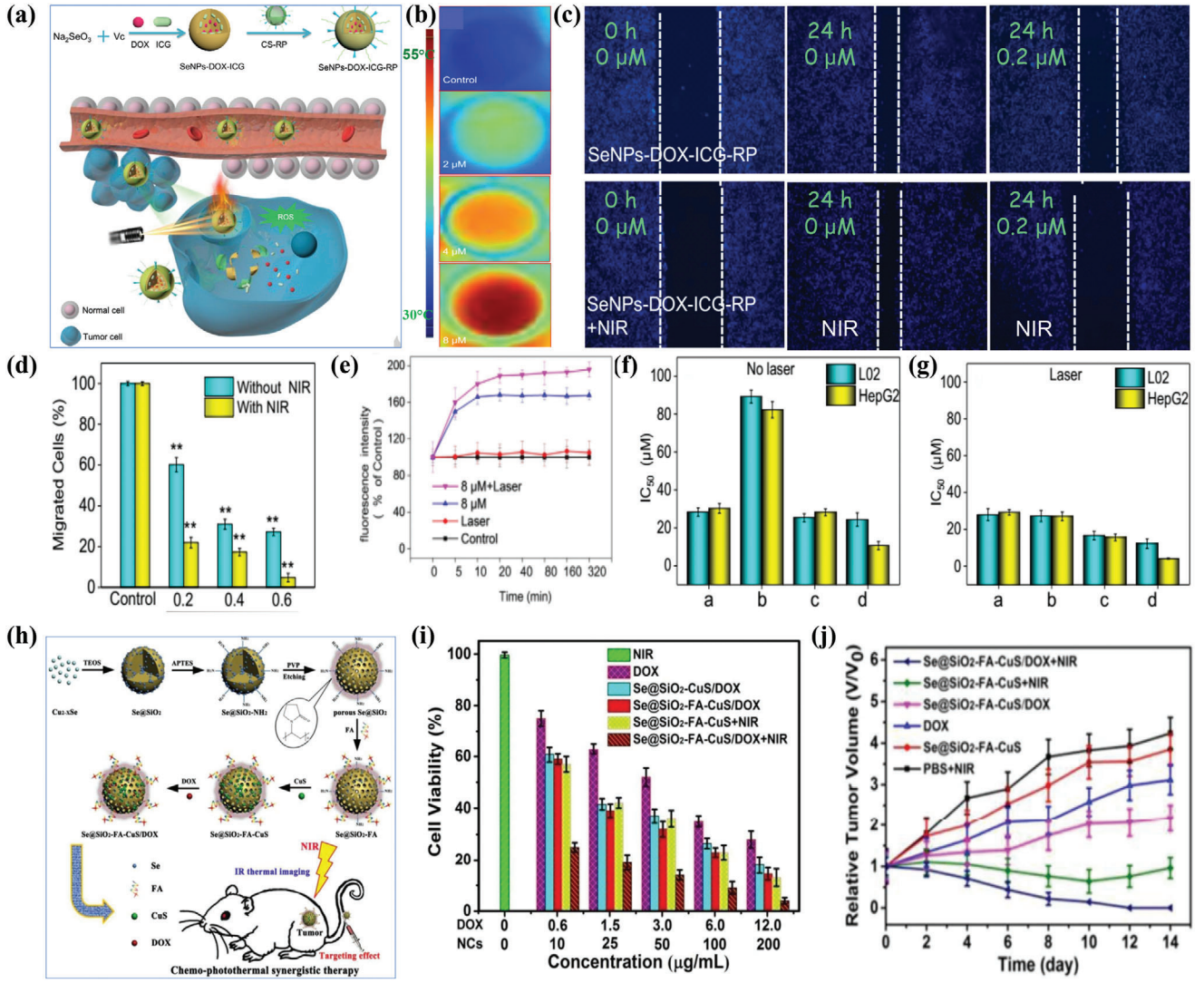

Figure 10. Chemo-photothermal therapy with nano-Se. a) Schematic showing the 0D nano-Se-based delivery system composed of nano-Se (nanocarrier as well as nanoagent), doxorubicin (DOX; drug), indocyanine green (ICG; photothermal [PT] agent),chitosan (CS)-bonded targeting ligands (RC-12 and PG-6 peptides) and the anticancer mechanism. b) Thermal images of HepG2 cells treated with nano-Se nanoparticles (SeNP)-DOX-ICG-RP under near infrared (NIR) irradiation. c) Migration behaviors of HepG2 cells treated with SeNP-DOX-ICG-RP at various concentrations and time points with or without NIR irradiation. d) Percentage of migrating cells under different treatments. e) NIR irradiation (808 nm, 3 W cm^{-2}, 2 min) effect on intracellular reactive oxygen species (ROS) levels in HepG2 cells treated with SeNP-DOX-ICG-RP. f,g) Anticancer activity of various nanoplatforms (a, SeNPs-DOX; b, SeNPs-DOX; c, SeNPs-DOX-ICG; d, SeNPs-DOX-ICG-RP) with or without NIR illumination. Reproduced with permission.[177] Copyright 2018, Wiley-VCH. h) Schematic showing the 0D ultrasmall nano-Se dot-based therapeutic nanoplatforms comprising nano Se dots (nanoagent), porous SiO_2 (nanocarrier), folic acid (FA; targeting molecule), CuS nanoparticle (PT agent) and DOX (drug) and a proposed combined dual-modal therapy against cancer. i) In vitro anticancer behaviors of various delivery systems (DOX, Se@SiO_2-CuS/DOX, Se@SiO_2-FA-CuS/DOX) under various conditions. j) In vivo anticancer activity reflected by changes in relative tumor volumes in tumor-bearing mice after various treatments. Reproduced with permission.[182] Copyright 2018, The Royal Society of Chemistry.

applied porous SiO_2 as a solid template to fabricated 0D nano-Se dots and loaded this with PTT agent copper sulfide nanoparticles (CuS-NPs) as well as DOX, leading to the formation of Se@SiO_2-FA-CuS/DOX nanocomposites (Figure 10h). The targeting ability of such a complex nanoplatform was achieved via folic acid (FA) with electrostatic absorption. The biocompatibility of Se@SiO_2-FA-CuS/DOX nanocomposites was investigated systematically. It was found that DOX alone demonstrated obvious cytotoxicity to normal human endothelial cells, indicating its side effects for normal tissues. However, it was interesting to find that with the same DOX concentration, the proposed Se@SiO_2-FA-CuS/DOX not only showed a lower toxicity towards normal cells but exhibited higher anticancer activity. The reason for the latter phenomenon was based on the dual chemotherapeutic effects of nano-Se and DOX. With the enhanced chemical therapeutic effect, Se@SiO_2-FA-CuS/DOX has been demonstrated to be strongly active against cancer cells in a DOX-loading or nanoplatform concentration-dependent manner (Figure 10i,j). It was also

noted that Se@SiO_2-FA-CuS under NIR illumination without addition of DOX also possessed favorable tumor inhibitory effect. However, after 10 days of treatment, the tumor relative volume was increased, indicating recurrence of tumor following PTT-chemotherapy with nano-Se (Figure 10j). This interesting investigation suggested the validity of a synergistic integration of nano-Se/drug/PTT agents to combat cancer.

3.4. Nano-Se + Nanotemplates

In addition to surface engineering strategies, integrating nano-Se with nano-templates has also been found to be effective in improving the anticancer capacity of nano-Se. **Figure 11** shows three typical nanotemplates described in the literature, namely organic polymer-based nanofiber, inorganic TiO_2 and anodized aluminum oxide (AAO) nanotemplates. In 2017, Zhang's group[194] reported highly stable nano-Se embedded in polysaccharide-based hollow nanofibers. They adopted a highly branched glucan polysaccharide (AF1) as a polymer matrix which showed strong self-assembly ability to form hollow nanofibers in water (Figure 11a). An in situ reduction reaction process for Se in the presence of this AF1 polymer can produce nano-Se-embedded AF1 nanofiber (Se-AF1) structures (Figure 11b) with a homogeneous dispersion of 0D Se within the nanofiber matrix, leading to excellent stability (up to 18 months), superhigh biocompatibility and minimal side effects of Se NPs. Furthermore, the AF1 nanofiber could effectively enhance the cellular uptake of Se NPs, shown in the fluorescence images in Figure 11c. It is also interesting to find that Se-AF1 showed a synergistic anticancer effect on a broad spectrum of cancer cells, especially for MCF-7 with a rather low IC_{50} value of 33 μg mL^{-1} and a corresponding Se concentration of only 4.8×10^{-6} M (Figure 11d). Western blotting analysis indicated that Se-AF1 could induce apoptosis of tumor cells in a mitochondria-mediated apoptotic pathway, with downregulation of poly(ADP-ribose) polymerase (PARP1) and Bcl-2, and expression of programmed cell death protein 4 (PDCD4) (Figure 11e). As a result, compared with AF1 alone, Se-AF1 can significantly inhibit the growth of solid tumors (Figure 11f). Conversely, for bone cancer, inorganic implants are frequently needed. These should meet requirements such as good mechanical properties and antiinflammatory, biocompatibility, and anticancer bioactivity. In this regard, nano-Se combined with inorganic nanotemplates is promising. In 2012, Chen et al.[195] reported Se-deposited and chitosan-coated TiO_2 nanotube substrates (TiO_2 nanotube-Se-Chi) generated by an electrodeposition method, shown in Figure 11g. The anodization can induce TiO_2 nanotube arrays with an average diameter of about 110 nm and a length of around 900 nm (Figure 11h). After the deposition process, discernable layers of Se or Se NPs cannot be observed, shown in Figure 11i, likely because the deposited Se substance is too little to be distinguished from the wells of TiO_2 nanotube arrays. It was also found that TiO_2 nanotubes showed adverse effects on healthy osteoblast cell adhesion with less spreading morphologies observable (Figure 11j). However, when the nano-Se was deposited onto TiO_2 nanotubes (Figure 11k), osteoblasts displayed increased spreading morphologies, which can be further improved in the case of nano-Se-deposited and chitosan-coated TiO_2 nanotubes shown in Figure 11l. Furthermore, the nano-Se-deposited and chitosan-coated TiO_2 nanotubes exhibited strong inhibition of cancerous osteoblasts, as shown in Figure 11m, indicating their promising anticancer capacity. In 2015, Saji et al.[196] reported a Se/AAO-based localized drug delivery system for bone implants. In their study, several kinds of Se, including inorganic Se (H_2SeO_3; HA), organic Se [$(C_6H_5)_2Se_2$] (DPDA), metallic Se (Se) (Se metallic), electrodeposited Se (ED Se) and chemical vapor deposited Se (CVD Se), were employed to load the nanoporous AAO templates (Figure 11n). For polymer modification with chitosan, both HA and DPDA showed a film-like structure inside the pore walls, indicating their infiltrating behaviors within AAO templates when compared with those without chitosan modification (Figure 11o). Both ED- and CVD-based nano-Se could be observed with an inhomogeneous distribution onto AAO porous networks (Figure 11o). Furthermore, a decreasing anticancer effect against a human osteosarcoma cell line in the order of HA-chitosan > ED Se > CVD Se > metallic Se-chitosan > DPDA-chitosan was found, which suggested that nano-Se (ED Se, CVD Se and metallic Se) has a compromised anticancer capacity within AAO templates when compared with inorganic selenite (HA).

4. Nano-Te for Strong Anticancer Treatment

Belonging to the same group in the periodic table, Te and Se in their crystalline forms have very similar features, such as similar preparation methods for obtaining 2D morphological nanosheets, similar crystal parameters, and similar anticancer capacities. However, the literature has demonstrated an obvious difference between nano-Se and nano-Te. For instance, being a semiconductor with narrow energy bandgap, nano-Te has been found to have excellent photointermediate biomedical applications, including PTT, PDT, and photoacoustic imaging (PI). Yet, these features cannot be readily observed or reported for nano-Se. Conversely, nano-Te does not demonstrate any obvious damage to cancer cells in the absence of light stimulation, whereas nano-Se does exert its anticancer capacity without any external stimuli. Therefore, despite being in the same elemental group and possessing several similar optoelectrical properties, the mechanisms by which nano-Te and nano-Se combat cancer cells are different and unique. A deep analysis and understanding of their molecular mechanisms will guide more powerful anticancer strategies, taking advantage of combining the properties of nano-Se and nano-Te in the future.

4.1. 1D-Te for Chemotherapeutic Agents

Following previous works concerning the antioxidation and anticancer effects of nano-Se, nano-Te, generated from the monoelement Te, positioned directly below Se in the periodic table, has also demonstrated promise for anticancer applications. Huang et al.[197] first reported this pioneering work in 2016, starting from a case of 1D Te-nanorods with surface modification using polysaccharide–protein complex extracted from *Pleurotus tuber-regium* (PTR; **Figure 12**a). Without the PTR modification, nano-Te occurred in the 1D form of nanowires with unfavorably long lengths (Figure 12a). Incorporating the PTR polymer into the Te redox reaction system, Te nanorods with significantly shortened

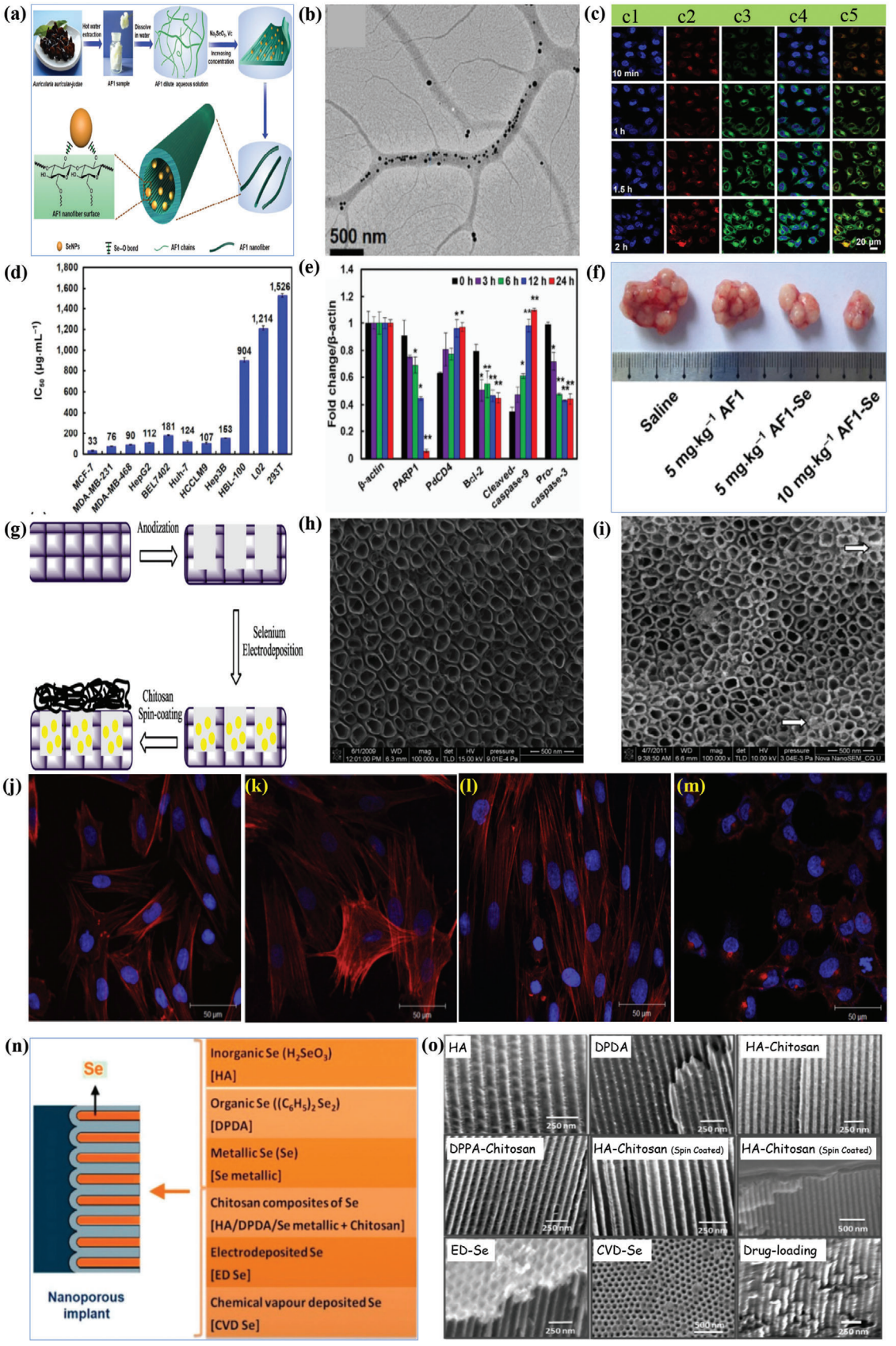

lengths and PTR surface modification were obtained (Figure 12a). It was found that Te nanowires (TeNWs) without PTR decoration exhibited unfavorable hemocompatibility when cultivated with human erythrocyte cells. As shown in Figure 12b, compared with the control PBS group, the naked Te-nanowire-treated group exhibited an obvious morphology change in erythrocyte cells. However, PTR-coated Te nanorods (PTNRs) did not alter erythrocyte morphology. Additionally, they also caused lower hemolysis of erythrocytes compared with TeNWs regardless of time or concentration. It was also found that PTNRs had excellent anticancer selectivity and activity in vitro. For instance, they had higher antiproliferative effect on various types of cancer cells, including MCF-7, A549, A375, HepG2, and Neuro-2a cells but significantly lower effect on normal HK-2 cells. MCF-7 cells had been reported to possess the lowest IC_{50} value of 5.52 ± 0.89 μg mL^{-1} in this investigation, and growth was inhibited by PTNRs in a concentration-dependent manner (Figure 12c). The authors also further showed that apoptosis was the main mechanism responsible for the Te anticancer effect due to an increase in Sub-G1 value with increasing Te concentration, accompanied by DNA fragmentation and nuclear condensation (Figure 12d). Importantly, it was also observed that increasing PTNR dose resulted in significant loss or depletion of $\Delta\psi_m$ in MCF-7 cells (Figure 12e), strongly suggesting that PTNRs caused mitochondria dysfunction in MCF-7 cells and that $\Delta\psi_m$ was involved in induction of cell apoptosis. Such a phenomenon is very similar to that of nano-Se.

In 2019, a nano-Te "pro-drug" concept was proposed by Wu et al.[198] for the first time. It is well known that the tumor microenvironment has unique characteristics, such as abundant concentrations of hydrogen peroxide (H_2O_2) and GSH. For instance, the H_2O_2 concentration can be up to 100×10^{-6} M in cancer cells, significantly higher than the 20×10^{-9} M found in normal cells. Considerable changes in H_2O_2 concentration, either increase or decrease, can cause cancer cell apoptosis. Besides, from a functionality point of view, a decrease in GSH content can result in increased ROS levels, further facilitating killing of cancer cells. Considering this situation, the authors believed that Te-based nanostructures may react with H_2O_2 to produce highly toxic TeO_6^{6-} and that these TeO_6^{6-} ions can sequentially react with GSH within tumor cells, via the following two reaction pathways

$$Te + 3H_2O_2 \rightarrow 6H_6TeO_6 \quad (4)$$

$$nGSH + TeO_6^{6-} \rightarrow GS - Te - GS + GSSG \quad (5)$$

The above two reactions can result in considerably decreased levels of both H_2O_2 and GSH, and the subsequent enhancement of ROS in the tumor (**Figure 13**a).Their results showed that TeNWs of about 80 nm in length and 6 nm in width can selectively kill tumor cells (MCF-7, A549 and HeLa cancer cell lines) and had no significant influence on the cell viability of HSF and L02 normal cell lines (Figure 13b). It was further investigated that within the above-mentioned cancer cell lines, H_2O_2 levels were significantly decreased when cultivated with TeNWs and that this phenomenon did not occur in the normal cell lines (Figure 13c). Confocal fluorescence microscope images (Figure 13d) of MCF-7 cells further confirmed the decrease of H_2O_2 concentration with an obviously decreased fluorescence signal intensity after TeNW treatment. Interestingly, it was also found that TeNWs caused cleavage of DNA within the nucleus, which is responsible for cancer cell apoptosis. Further, the authors highlighted that both toxicH_6TeO_6 and increased ROS could explain the DNA damage and that the generated H_6TeO_6 was the main contributor. Additionally, the TeNWs, coated with BSA and dextran conjugate (BSA–dextran), could be dissociated into small molecules to be removed from body, suggesting only minor side effects (Figure 13e). It was also noted that except for favorable tumor growth inhibition, no significant inflammation, or infection were observed in treated mice.

4.2. Light-Mediated Synergistic Therapy Against Cancer

Both Te and Se crystals are semiconductors with broad optical absorption, implying potential light-mediated synergistic therapy against cancer. Despite the similar physical optoelectrical properties of nano-Se and nano-Te, recent investigations have demonstrated the potential application of nano-Te-based nanoplatforms only in this field.

4.2.1. PTT+PDT

In 2017, the intriguing photo-induced synergistic cancer therapy application of nano-Te in the form of nanodots was reported for the first time by Yang et al.[144] Therapeutic characteristics must be met for inorganic nanoparticles used in biomedical applications, such as biocompatibility (largely dependent on the biological stability of the nanoparticle in question, in particular the highly toxic features of high-valence ion forms), cancer-targeting ability (dependent on, for example, surface engineering,

Figure 11. Nano-Se-integrated nanotemplates with novel anticancer activities. a) Nano-Se incorporating a highly branched polysaccharide (AF1) into self-assembling composite nanofibers (AF1-Se). b) Transmission electron microscope image showing branched polymer nanofibers with embedded 0D nano-Se. c) Fluorescence images showing intracellular trafficking of AF1-Se (c1: Hoechst 33342; c2: Lyso tracker; c3: AF1-Se; c4: overlay of H-33342 + AF1-Se; c5: overlay of Lyso+AF1-Se) at indicated time points. d) Anticancer activity of AF1-Se towards a broad spectrum of cancer cell lines including human breast adenocarcinoma cell lines (MCF-7, MDA-MB-231, and MDA-MB-468) and human hepatocellular carcinoma cell lines (BEL7402, Huh-7, HCCLM9, HepG2, and Hep3B). Note that cell lines HBL-100, L02, and 293T are noncancer human lines. e) Expression behaviors of proteins induced by AF1-Se at various time points. f) Solid tumors obtained from saline- and AF1-Se-treated mice. Reproduced with permission.[194] Copyright 2017, Springer Nature. g) Nano-Se deposited and chitosan-coated TiO_2 nanotubes arrays. h) Field-emission scanning electron microscopy (FE-SEM) image of top view of TiO_2 nanotubes. i) FE-SEM image of top view of nano-Se-deposited TiO_2 nanotubes. j–l) Morphologies of healthy osteoblasts cultured onto TiO_2 nanotubes, nano-Se-deposited TiO_2 nanotubes and nano-Se-deposited and chitosan-coated TiO_2 nanotubes, respectively. m) Morphology of cancerous osteoblasts cultured onto nano-Se-deposited and chitosan-coated TiO_2 nanotubes. Reproduced with permission.[195] Copyright 2013, Elsevier B.V. n) Anodized aluminum oxide (AAO) as a model nanoporous drug delivery carrier for loading various kinds of nano-Se as well as its counterparts including inorganic Se-based salts and organic Se. o) SEM images showing the nature of Se and drug loading in AAO. Reproduced with permission.[196] Copyright 2015, The Royal Society of Chemistry.

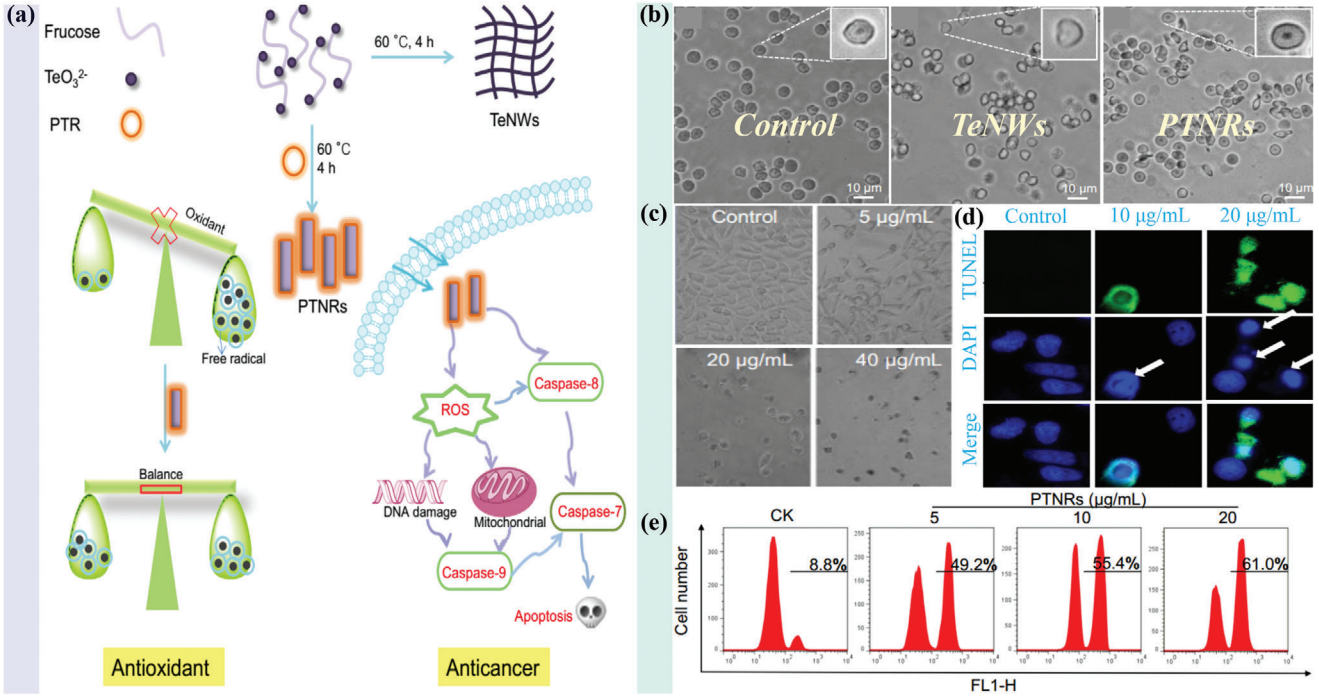

Figure 12. The first demonstration of nano-Te alone for tumor inhibition. Reproduced with permission.[197] Copyright 2016, Wiley-VCH. a) Mechanisms of preparation, surface modification, and anticancer activity of 1D Te nanorods (TeNRs). b) Hemocompatibility evaluation, reflected by morphologies of erythrocyte cells incubated with PBS solution (control), naked Te nanowires (TeNWs) and polysaccharide–protein complex extracted from *Pleurotus tuber-regium* (PTR)-modified Te nanorods (PTNRs). c) Anticancer activity evaluation showing the cytotoxicity of increasing concentrations of PTNRs on MCF-7 cancer cells. d) MCF-7 cell apoptosis induced by treatment with PTNRs at various concentrations using TUNEL and DAPI staining. e) Mitochondrial dysfunction caused by PTNRs with a significant loss of mitochondrial transmembrane potential ($\Delta\psi_m$).

surface chemistry or charge, and microscopic dimensions), post-treatment metabolism (such as renal excretion), and low adverse side effect profile. To meet these requirements for nano-Te, Yang et al., fabricated ultrasmall Te-nanodots within HSA as a nanoreactor. In fact, these HSA-encapsulated Te nanodots resulted in the double effect of HSA surface modification and as a semiconductor with quantum dimensions. The former is associated with cellular uptake and biocompatibility, thus playing an important role in therapeutic effect, and the latter is strongly correlated with physical optical properties, which can be responsible for the final PTT and/or PDT effects. As shown by Yang et al.[144] in **Figure 14**, Te nanodots simultaneously possess excellent photothermal and photodynamic characteristics under single NIR irradiation with a wavelength of 785 nm (Figure 14a). As a typically semiconductor, NIR irradiation can compel Te to produce a transition excitation behavior from valence band to conduction band, giving rise to electron–hole pairs (EHP). The EHP, on the one hand, relaxed heat energy via a nonradiative mechanism to confer photothermal effect, and on the other hand, reacted with oxygen within the tumor site (despite its extremely low concentration) to produce ROS, such as superoxide radicals ($\bullet O_2^-$) and subsequent dismutated hydroxyl radicals ($\bullet$OH) (Figure 14a). As a result, Te nanodots showed a photo-induced synergistic PTT and PDT (Figure 14a). Nano-Te dots had a photothermal conversion efficiency of 40.0% (Figure 14b) and exhibited a robust photothermal stability (Figure 14c). In addition, nano-Te dots were able to generate ROS with types of $\bullet O^{2-}$, and $\bullet$OH (Figure 14d), indicating that nano-Te dots undergo a type-I mechanism to produce highly reactive ROS under NIR light illumination.

As shown in Figure 14e, the IC_{50} values of PTT alone (adding vitamin C to scavenge ROS to exclude the effect of PDT), PDT alone (under low temperature experimental conditions of 4 °C, to exclude the effect of PTT) and PTT + PDT were reported to be 0.38×10^{-3}, 0.69×10^{-3}, and 0.17×10^{-3} M, respectively, in vitro indicating a synergistic index of 0.69.Additionally, the PDT effect of Te-nanodots was also proven in vivo by dihydroethidium staining in Figure 14f, which is a prerequisite condition for clinical PDT efficacy. In vivo, the synergistic effect of PTT and PDT was also demonstrated (Figure 14g). The results showed that PTT alone could not ablate all tumors but that combined therapy with PTT and PDT at a threshold injection dosage of 12.5 μmol kg^{-1} completely destroyed all tumors (Figure 14h). Hematoxylin and eosin staining of tumor sections from the nano-Te-dot-treated mice at 6 h postirradiation showed that nano Te dots under irradiation caused destructive damage to the tumor while PBS with or without light irradiation did not induce detectable tumor damage (Figure 14i). Furthermore, no significant changes of serum biochemistry (Figure 14j,k) were observed, indicating promising hemocompatibility and biosafety of Te nanodots. The authors also noted that when the injection dosage was increased to 50.0 μmol kg^{-1}, accompanied by a considerably lower irradiation power density, 0.35 W cm^{-2}, excellent tumor ablation was achieved.

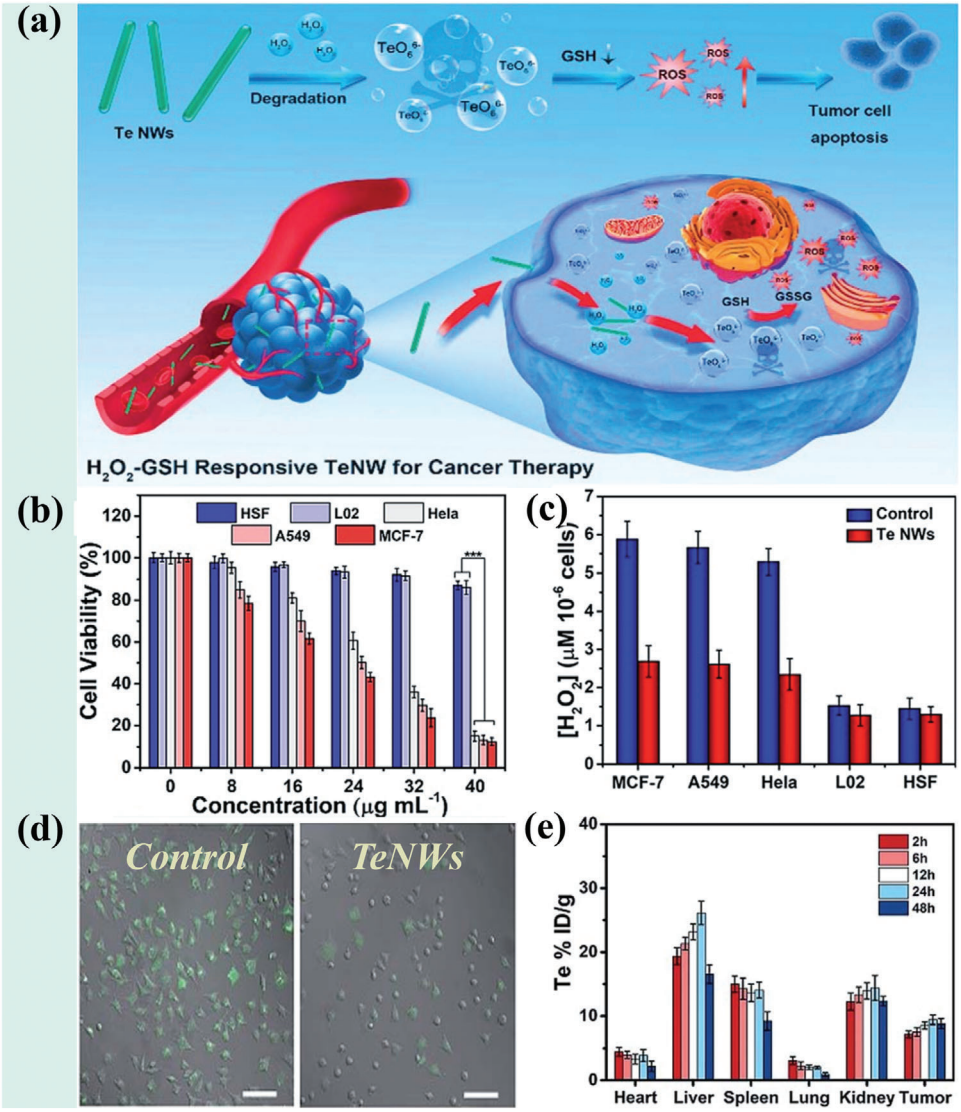

Figure 13. Prodrug demonstration of nano-Te for selective cancer therapy. Reproduced with permission.[198] Copyright 2019, The Royal Society of Chemistry. a) Schematic showing H_2O_2– then glutathione (GSH)-activated 1D Te nanowires (TeNWs) for highly selective tumor treatment. b) Assessment of anticancer activity and selectivity between cancer and normal cells. The cancer cell lines used included MCF-7 (human breast cancer), HeLa (human cervical cancer) and A549 (human lung cancer), and normal cell lines wereL02 (normal human liver cells) and HSF (human skin fibroblasts). c) Changes in intracellular H_2O_2 concentration after co-incubation of different cell lines with TeNWs. d) Confocal fluorescence microscope images of MCF-7 cells after differing treatments for 6 h. e) Biodistribution of elemental Te in major organs and tumors.

4.2.2. 2D Te for PI-Guided PDT

In 2018, Lin et al.[146] first reported the anticancer PI performance and PDT of nano-Te in the form of 2D geometry. Unlike most nano-Te structures originating from a chemical reduction approach, Lin et al. following the work of Xie et al.,[151] synthesized small sized 2D Te nanosheets by means of LPE starting from crystalline Te powders (**Figure 15**a). To improve chemical stability as well as biocompatibility, 2D Te nanosheets were first functionalized by GSH prior to use. It was found that, under 670 nm wavelength illumination, 2D Te nanosheets could effective generate singlet oxygen ($^1O_2$) by oxidizing oxygen (O_2) via a type-II mechanism, which is different from that of a type-I mechanism for Te nanodots mentioned above. Merged confocal fluorescence microscopy images of HeLa cells in Figure 15b using dichlorofluorescin diacetate as a fluorescent probe demonstrated a distinct intracellular ROS production within HeLa cells under 670 nm light irradiation in the presence of 2D Te@GSH, indicating good PDT behavior of 2D Te nanosheets. The cell viability of 2D Te@GSH-treated HeLa cells was also evaluated using fluorescence microscopy in Figure 15c. It was found that under 670 nm light illumination 2D Te@GSH also caused significant damage to HeLa cells, suggesting a potential PDT application of 2D Te nanosheets for cancer treatment. The PI capacity of nano-Te was demonstrated in this study for the first time. In aqueous solutions, as shown in Figure 15d, the photoacoustic signal

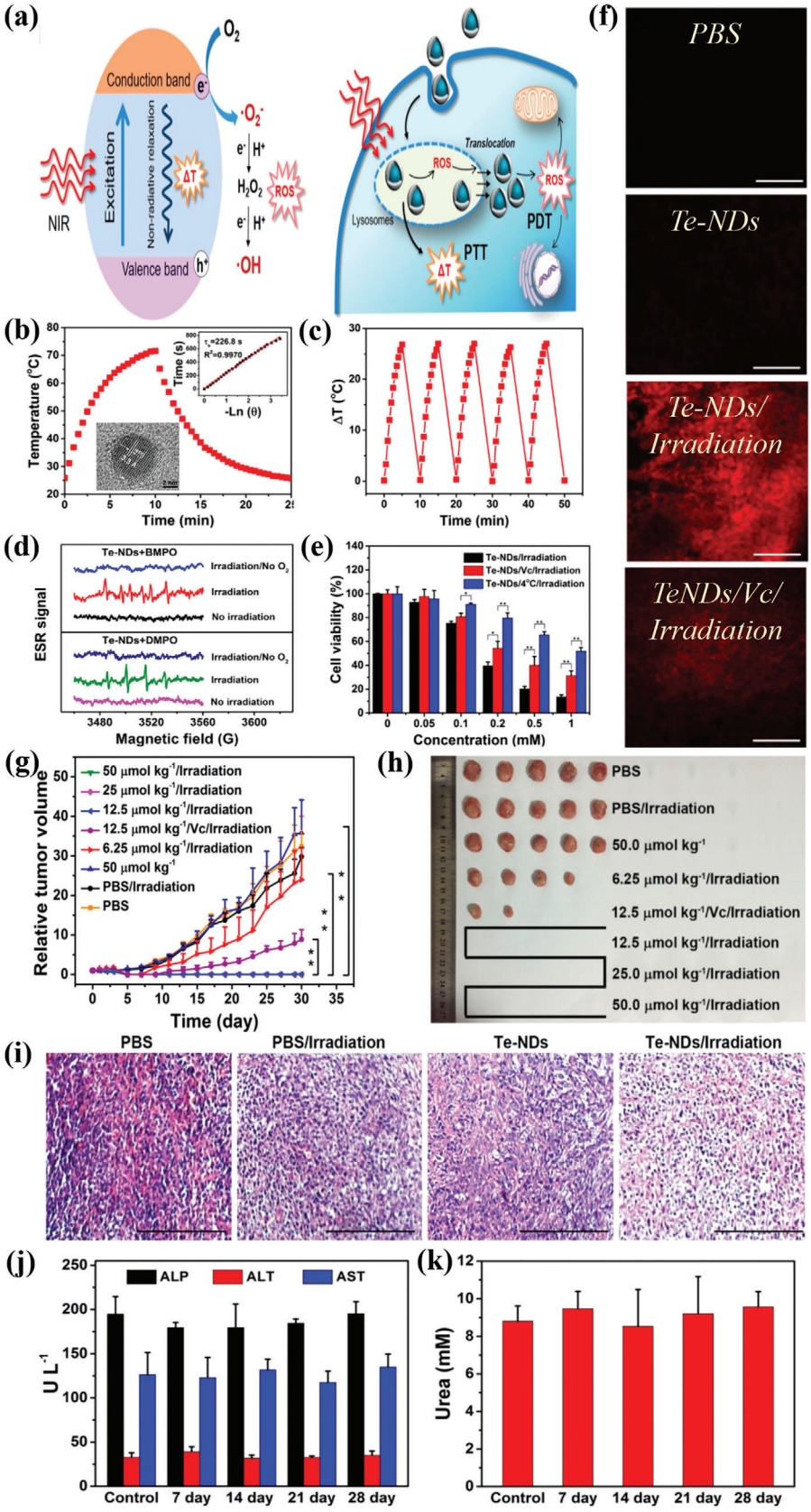

intensity of 2D Te nanosheets increased as their concentration increased, suggesting potential use as a PI contrast agent. In addition to this intriguing photoacoustic property, 2D Te nanosheets were found to be effective in vivo for PI (Figure 15e), with a significant increase of photoacoustic intensity at the tumor site after intravenous administration. This phenomenon also proved that effective accumulation of 2D Te nanosheets in the tumor occurred, probably due to enhanced permeability resulting from the GSH modification. In vivo, the 2D Te nanosheets had an efficient PDT effect on inhibiting tumor growth under irradiation, compared with other control groups, as shown in Figure 15f,g.

It is noteworthy that naked 2D Te nanosheets without any modification with biomaterials or natural resources are unstable in water, probably degrading into various types of Te-based ions, with an obvious color change of the aqueous solution. In addition, Te-based anions, such as tellurate (TeO_4^{2-}) and tellurite (TeO_3^{2-}) are highly toxic. Under this circumstance, an important open question remains: what toxicity and biocompatibility can naked but stable nano-Te offer? In other words, is it possible that undecorated but stable nano-Te may show biocompatibility similar to polymer- or bio-macromolecule-modified nano-Te? Addressing this point will be important in the future to evaluate the biosafety of Te-based nanomaterials for biomedicine.

4.2.3. PTT +Chemotherapy

A 2016 study demonstrated that nano-Te itself, an inorganic nanoparticle, showed intriguing anticancer activity with unique molecular mechanisms, by which it totally differed from classic organic anticancer drugs.[199] At this point, nano-Te can be regarded as a chemotherapeutic agent, superior and distinguished from other well-known previously reported inorganic materials, such as GO, BP and MXene[126] that do not provide any anticancer capacities without light illumination. Along with its excellent optoelectrical properties, nano-Te can be readily designed as a combined nanoplatform comprising anticancer chemotherapy and PTT. In 2017, Chen's group first reported one such interesting combination therapy for combating cancer, starting from the design of chemically synthesized Te nanoparticles (TeNPs) and polysaccharide–protein complex-decorated TeNPs (PTW-TeNPs) (**Figure 16**a). Several interesting results were achieved: 1) unique anticancer activity, from a chemotherapy point of view. PTW-TeNPs possessed excellent selectivity between cancer and normal cells, and anticancer activity, especially in HepG2 cancer cells (Figure 16b). Subsequently, this anticancer activity of PTW-TeNPs was shown to be concentration-dependent, which was further enhanced by laser illumination (Figure 16b). It seemed that PTW-TeNPs were superior to naked TeNPs in killing cancer cells. Additionally, the anticancer activity of nano-Te originated from ROS overproduction that could be further enhanced by laser irradiation (Figure 16c). It was also found that higher cellular uptake of PTW-TeNPs than that of TeNPs was likely responsible for the better anticancer capacity, which was due to the surface modification by polysaccharide–protein complex. 2) Excellent photothermal properties. The results shown in Figure 16d show that PTW-TeNPs had a photothermal conversion efficiency (η, 808 nm) of 37.4%, higher than other reported inorganic photothermal materials. The above two properties of nano-Te have the potential to facilitate building of a combined nanoplatform of chemotherapy and PTT against cancer. The MR imaging in Figure 16e further confirmed the strong anticancer effect of nano-Te and favorable healing capability at day 21 post-treatment. 3) Excellent therapeutic effect of the chemotherapy plus PTT combination (Figure 16f). It was noted that in this study, an 808 nm wavelength light with a high power density of 3 W cm^{-2} was employed to initiate photothermal behaviors of nano-Te. In fact, under this illumination, the overproduction of ROS within cells was further enhanced, as shown in Figure 16c. Therefore, it is hard to ignore the PTT effect on inhibiting tumor growth. As a result, an effective nano-Te combined therapy against cancer can be made up of chemotherapy, PTT and PDT.

4.2.4. Chemotherapy + PA +PTT

Following the earlier work of Chen and colleagues, in 2018 Yu et al.[145] reported blue Te-nanoneedles as "all-in-one" nanoagents for synergistic thermo-chemotherapy of tumors. The reported 1D PVP-modified Te nanoneedles, reduced by GSH, showed good selectivity between the normal cell line, L02, and cancer cell lines, MCF7, HCT116, and H1299 at 48 h (**Figure 17**a). Furthermore, it was also found that Te nanoneedles had an excellent selectivity among cancer cells (Figure 17a). When cultured with Te nanoneedles, MCF7 cell numbers decreased with increasing Te-nanoneedle concentration (Figure 17b), losing normal morphology at the highest concentration of 60 mg L^{-1} (Figure 17b). The loss of $\Delta\psi_m$ in MCF7 cells gradually increased from 2.52% (normal) to 13.1% at 10 mg L^{-1} and 64.5% at 30 mg L^{-1} (Figure 17c), which resulted in mitochondrial dysfunction to further induce cell apoptosis. The fluorescence images in Figure 17d clearly show the increasingly fragmented dots of mitochondria as

Figure 14. Synergistic nano-Te-based photothermal therapy (PTT) and photodynamic therapy (PDT) combination therapy against cancer. Reproduced with permission.[144] Copyright 2017, American Chemical Society. a) Schematic illustration of mechanisms of generating simultaneous photothermal effect and reactive oxygen species (ROS) by 0D nano Te dots (left) and intracellular synergistic PTT and PDT treatments (right). b) Photothermal property (inset: high-resolution transmission electron microscope image of a single nano Te dot) and c) photothermal stability of nano Te dots under 785 nm irradiation at 1.5 W cm^{-2}. d) Electron spin resonance (ESR) spectra of nano Te dots with or without molecular oxygen upon 785 nm irradiation at 1.5 W cm^{-2} using 2,2,6,6-tetramethylpiperide (TEMP), 5-tertbutoxycarbonyl-5-methyl-1-pyrroline N-oxide (BMPO), and 5,5-dimethyl-1-pyrroline-N-oxide (DMPO) as the spin-trapping agents of singlet oxygen ($^1O_2$), superoxide radicals ($\bullet O^{2-}$), and hydroxyl radicals ($\bullet$OH), respectively. e) Anticancer activity assessment of nano Te dots in cancer treatment models of PDT and PTT (Te NDs/irradiation), PTT alone (Te NDs/Vc/irradiation; Vc was used to eliminate the ROS induced by nano-Te-PDT behavior), and PDT alone (Te NDs/4 °C/irradiation) under a constant low temperature of 4 °C. f) Dihydroethidium (DHE) staining of tumor sections from nano-Te-dot-treated mice with or without the ROS-scavenger Vc, to determine the generation of ROS in vivo. g,h) In vivo anticancer effects of nano-Te based treatment platforms and respective tumors. i) Hematoxylin and eosin (H&E) staining of tumor sections from the nano-Te-dot-treated mice at 6 h post-irradiation. j) Blood levels of ALP, ALT, AST. k) Urea levels from mice treated with nano-Te dots at a single dose of 50.0×10^{-6} M kg^{-1} Te, at the indicated times post-treatment.

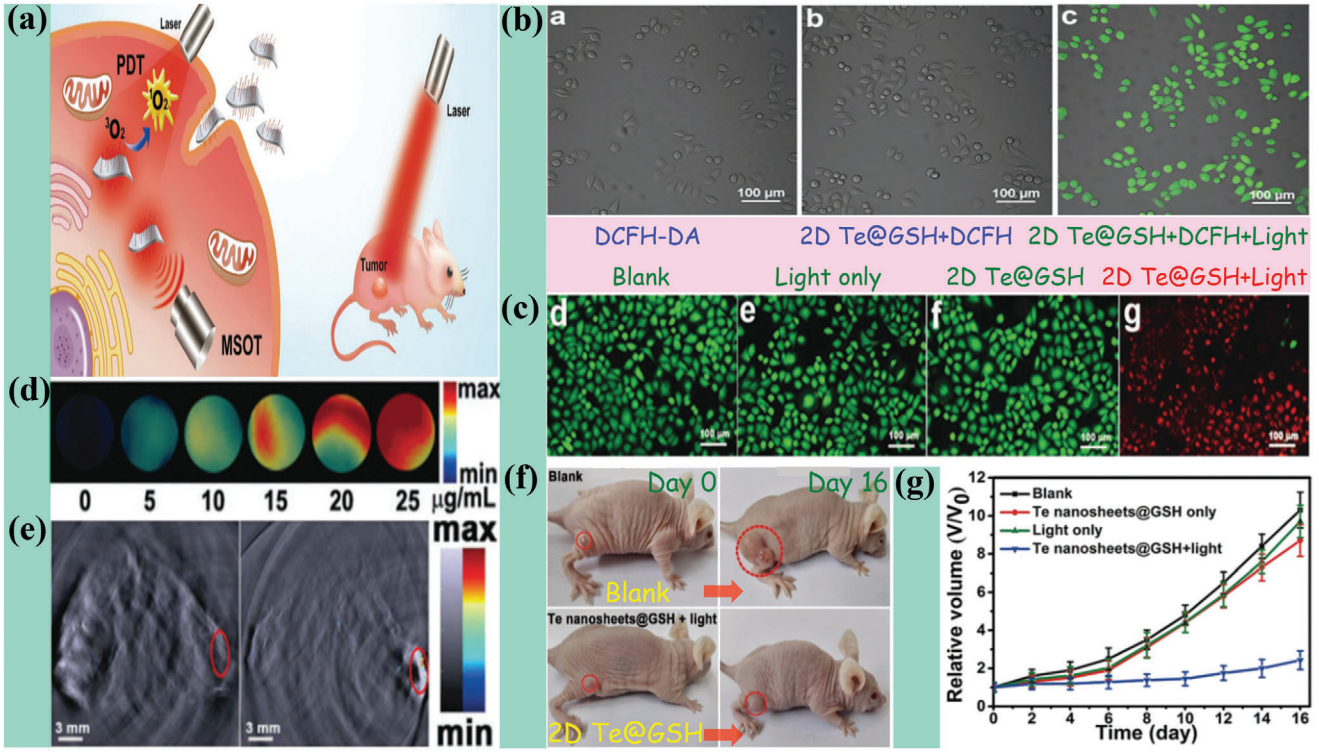

Figure 15. Photoacoustic (PA) imaging-guided photodynamic therapy (PDT) treatment of nano-Te. Reproduced with permission.[146] Copyright 2018, The Royal Society of Chemistry. a) 2D glutathione (GSH)-modified Te-nanosheet (2D Te@GSH)-based multispectral optoacoustic tomography (MSOT) and PDT against cancer. b) Merged confocal fluorescence microscopy images of HeLa cells after incubation with dichlorofluorescin diacetate (DCFH-DA), 2D Te@GSH+DCFH, and 2D Te@GSH+DCFH under light irradiation (670 nm, 160 mW cm^{-2}). c) Merged inverted fluorescence microscopy images of HeLa cells with differing treatments as indicated. The light irradiation conditions were wavelength, 670 nm; power density, 160 mW cm^{-2}; duration, 10 min. d) PA images of 2D Te@GSH solution of various concentrations. e) In vivo MSOT images of mice in the tumor region before and after the injection of 2D Te@GSH solution (20 μg mL^{-1}, 100 μL). f) HepG2 tumor-bearing nude mice before and 16 days after differing treatments. g) Relative volume of tumor in mice after differing treatments.

Te-nanoneedle concentration increased, confirming mitochondrial damage induced by Te nanoneedles. This study also demonstrated the promising PI capacity of Te nanoneedles due to their excellent photothermal effect. As shown in Figure 17e, a clear color comparison was observed after intratumoral injection of Te nanoneedles, suggesting validity of this treatment as an effective contrast agent. Encouraged by these favorable chemotherapy and PTT effects, Te nanoneedles were proven to effectively ablate tumors by a combined therapy model (Figure 17f). In vivo, the Te nanoneedles alone without light illumination demonstrated tumor growth inhibitory capacity to some extent (Figure 17g,h), again suggesting the unique chemotherapeutic effect against cancer. Augmenting the PTT effect significantly ablated solid tumors, as shown in Figure 17h.

5. Conclusions and Outlook

In the past two decades, inorganic nanomaterial-based nanomedicines have shown vibrant and powerful potential in the cancer treatment field. In the periodic table, three classic elements of Au, C and P have always dominated due to their individual mono-elemental nanostructures, such as ultrasmall Au NPs, GQDs, GO QDs, GO NSs, BP QDs and BP NSs. These unique nanomaterials, together with appropriate and rational surface modification or recombination, have the capacity to fight malignant tumors by serving as multifunctional nanodelivery systems. Three main intrinsic reasons can explain their promising biomedical applications. One is their specific geometrical shapes, that they are capable of being loaded with desirable drugs with a controllable release ability, genes, and other functional species. For instance, the ultrahigh specific areas of 0D quantum dots and 2D geometry nanosheets can be easily achieved. In this regard, BP QDs may be the best in view of their ultrasmall dimensions and wrinkled surface structures (i.e., anisotropy of BP). Second, excellent photo-mediated physical properties of Au-, graphene- and BP-based nanomaterials can confer these nanoplatforms with a promising light-mediated therapeutic efficacy against cancer. For example, Au NPs possess favorable surface plasma resonance under NIR irradiation to act as multifunctional PTT, PDT, photoacoustic, and MR agents. As a typical semiconductor with broad-spectrum absorption and tunable energy gap (E_p), BP has also been demonstrated to be powerful as a multifunctional nanoagent in the anticancer field. Finally, nanosized Au, graphene (or GO) and BP are desirably biocompatible and biosafe. In particular, BP has biodegradability characteristics with the relatively safe in vivo degradation product of phosphate, which is superior

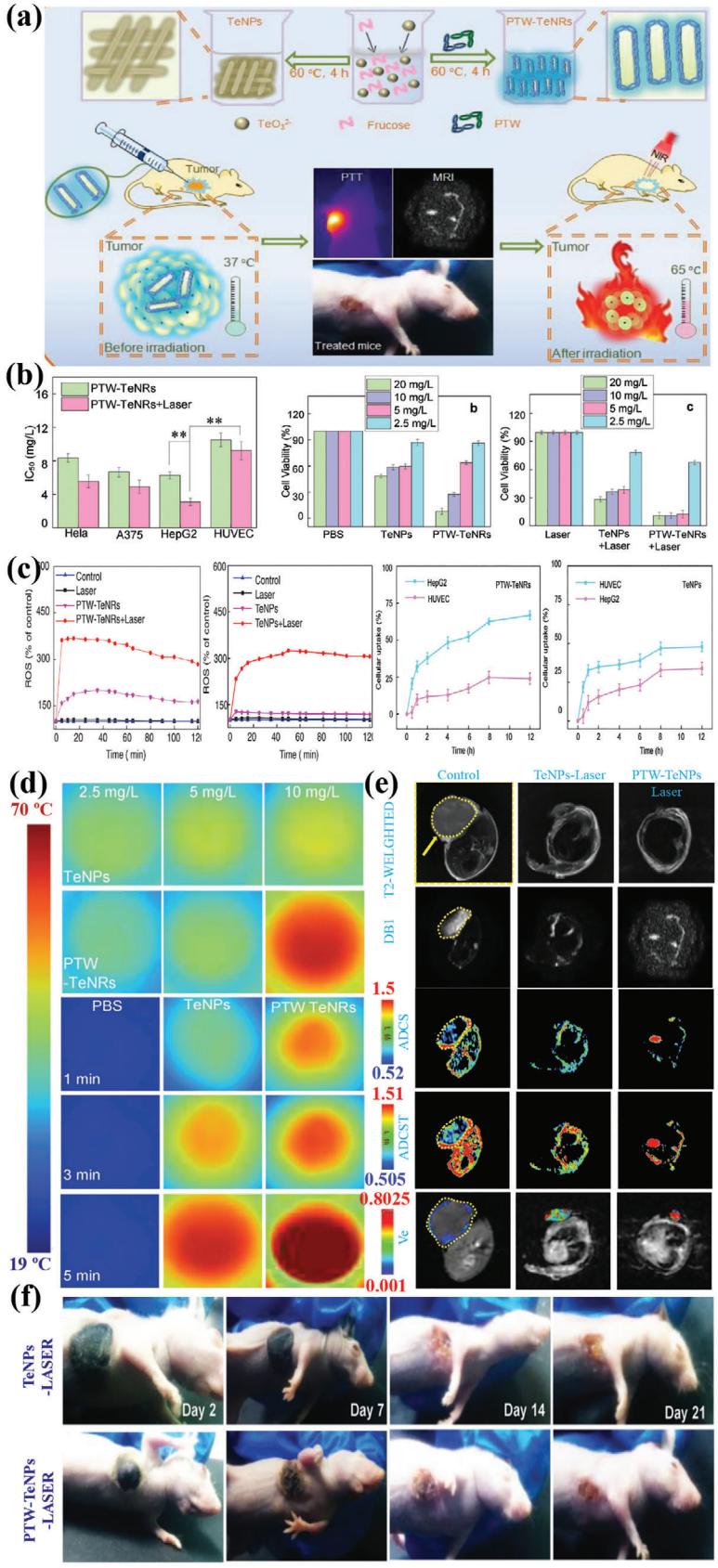

to that of other inorganic materials. Understanding of these three prerequisites of inorganic materials can aid further development of other nanomaterials for novel cancer therapy. For example, the Xene-based biomedical nanomaterials, such as MXene,[125–132] boron[200] and antimony,[87–89] can be considered to be spontaneous products under this development. However, it should be noted that these nanomaterials are not active against tumor cells and are also not involved in relevant bioactivities. Almost all investigations have shown that these nanomaterials have no selectivity between cancer and normal cells without light irradiation. In this regard, nano-Se and nano-Te have garnered significant attention with the additional advantage that they are bioactive for tumor cells as chemopreventive and chemotherapeutic reagents. Based on the above four reasons, this review has summarized nano-Se- and nano-Te-based multifunctional delivery systems for highly effective anticancer performance, including the elaborate nanostructure designs with different geometry morphologies, anticancer molecular mechanisms, and achievement of multi-modal cancer therapy by loading diverse species with or without NIR irradiation.

Highly active nano-Se-based biomedical nanoplatforms are dependent on appropriate and purposeful surface decorations. Compared with naked nano-Se, modified nano-Se systems have significantly improved chemical stability, biocompatibility, cellular uptake, selectivity between cancer and normal cells, tumor-targeting capability and thus anticancer activity as chemotherapeutic agents. These benefits can be acquired by, for example, loading biopolymers, targeting ligands, using small-molecule drugs, or using organic anticancer drugs. Furthermore, given their structural design plasticity originating from their chemical synthesis routes (undergoing nucleation and growth usually in the presence of template polymers and/inorganic nanomaterials), nano-Se-based platforms are usually based on nano-Se components in addition to others, such as genes, PT agents, inorganic materials and anticancer drugs. As a result, multifunctional combined therapy treatments can be achieved, such as chemo-gene therapy, chemo-PTT, chemo-radiotherapy and chemo-chemotherapy, in conjunction with NIR or X-ray irradiation. The synergistic therapeutic effects afforded by such combination therapies are considerably superior to those of nano-Se-based chemotherapy alone. It is noted that the photo-induced properties of nano-Se have not been strong and that their additional NIR-mediated therapy modes arise from the loading of other photosensitive nanomaterials, such as ICG and Cu_2S. Therefore, the self-anticancer activity of nano-Se is the foundation of these combined therapy modes.

The molecular mechanisms of nano-Se against cancer have been demonstrated to mainly involve cell apoptosis. Nano-Se can cause overproduction of ROS, DNA damage, mitochondrial dysfunction with depletion of $\Delta\psi_m$, and activation of caspase families with certain apoptosis signaling pathways, culminating in cell death. In addition, from a biomechanical point of view, the adhesion force and Young's modulus of the cell membrane of nano-Se-treated tumor cells were both significantly decreased, which also contributes to the death of tumor cells. As for nano-Te, it has a similar antioxidative ability to inhibit cancer cell proliferation. Unfortunately, insufficient investigations into the anticancer activity of nano-Te have been performed to fully understand the underlying mechanisms of action.

Owing to potentially greater metallicity than that of nano-Se, nano-Te-based nanoplatforms have usually been used as light-sensitive agents to combat cancer, except when in use as chemotherapy agents. Under NIR irradiation with a single light wavelength, nano-Te has the capacity to elicit simultaneous PTT and PDT effects. As a result, nano-Te-based nanoplatforms demonstrate combined PTT-, PDT-, or PTT–PDT-chemotherapy multi-modalities without the loading of any drugs. This benefit is quite distinct from those of BP, GO, Au and MXene, which are combined with additional drugs to achieve a chemotherapy-based anticancer combination therapy.

Considering its excellent and numerous evidence-based chemotherapeutic effects, nano-Se behaves like a kind of anticancer drug for cancer therapy. And as mentioned above, the nano-Se is not an effective NIR-mediated photosensitive reagent. Conversely, nano-Te is more inclined to act as a new kind of photosensitive reagent due to its outstanding photo-induced physical performances (PTT and PDT). It should be note that although the nano-Te has also been reported to have a capacity of chemotherapeutic effect more evidences and more profound investigations are needed to verify this point. Fortunately, it is reasonable to combine the nano-Se (chemotherapy) with the nano-Te (PTT, PDT, or the both) to build a more complex nanoplatform for cancer therapy. In addition, it is reported that Se- and Te-based crystals have a very high similarity deriving from their similar crystal cell parameters, which affords possibilities of combining Se with Te from a possible atom aspect. Very recently, for example, Chen et al. reported lateral Se-coated Te (TeSe) nanoheterojunctions for their excellent PTT performances for cancer treatment.[201] However, the obtained TeSe nanomaterials may not belong to neither nano-Se or nano-Te in view of the existence of Te–Se interfacial phases, which are not discussed in this review.

So far, numerous inorganic nanomaterials have been found and developed for cancer treatment. However, the size uniformity, biocompatibility, bioactivity, targeting ability, NIR-mediated photoresponsibility and metabolic process of these nanomaterials have not been well revealed, which are of great significance for their clinical applications. Furthermore, single one object is always not strong enough, which can be well reflected by loading extra chemical drugs, genes, proteins, and so forth. In this regard, a combination strategy may be promising to improve their

Figure 16. Synergistic nano-Te-based photothermal therapy (PTT) and chemotherapy combination therapy against cancer. Reproduced with permission.[199] Copyright 2017, Wiley-VCH. a) 1D Te-nanorods (TeNRs) with specific surface modification with mushroom polysaccharide–protein complexes (PTW; PTW-TeNRs), facile chemical synthesis and cancer therapy as a chemo-photothermal agent. b) Anticancer efficacy of TeNRs and PTW-TeNRs with or without laser irradiation. c) Reactive oxygen species (ROS) generation behaviors and cellular uptake behaviors of TeNRs and PTW-TeNRs with or without laser irradiation. d) Thermal images of HepG2 cells incubated with PTW-TeNRs or TeNPs at varying concentrations (808 nm, 3 W cm^{-2} and 5 min) and irradiation times (808 nm, 3 W cm^{-2}). e) Magnetic resonance images of HepG2 tumor-bearing mice after various treatments (PBS, TeNPs + laser and PTW-TeNRs + laser) on day 21. Tumor sites indicated by white dashed line. f) Representative photographs of typical mice treated with TeNPs or PTW-TeNRs under laser irradiation during 21 day observation period.

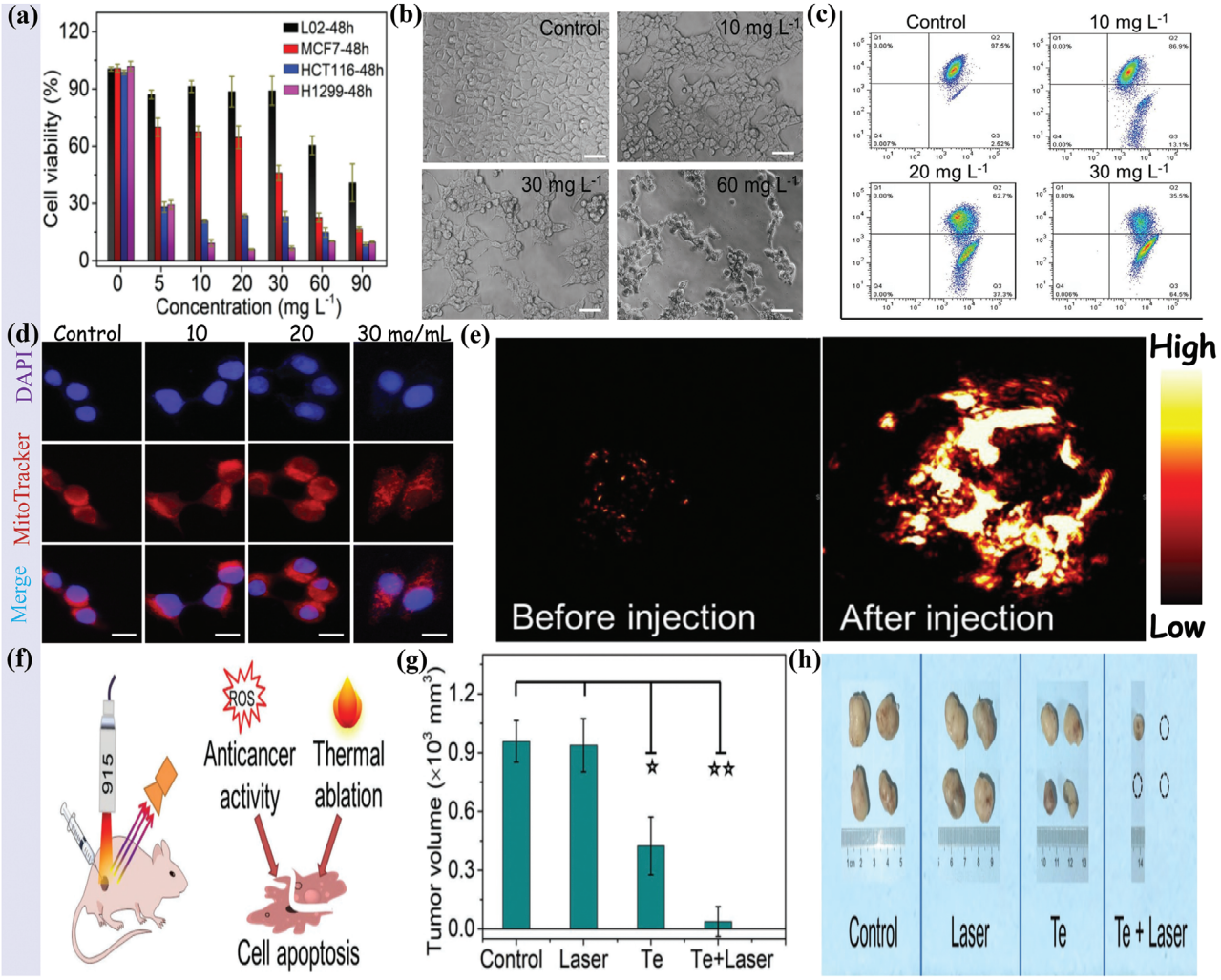

Figure 17. Synergistic nano-Te-based photothermal therapy (PTT)+photoacoustic (PA)+chemotherapy combination therapy against cancer. Reproduced with permission.[145] Copyright 2018, Wiley-VCH. a) Cell viability of normal cell line, L02, and cancer cell lines, MCF7, HCT116, and H1299, incubated with 1D Te nanoneedles at various concentrations for 48 h. b) Photomicrograph of MCF7 cells after cultivation with 1D Te nanoneedles at indicated concentrations, showing morphological changes in cells. c) Depletion of mitochondrial membrane potential in MCF7 cells treated with Te nanoneedles (10, 20, and 30 mg L^{-1}) using JC-10 mitochondrial probe. d) Typical images of mitochondrial rupture of MCF7 cells co-stained with the MitoTracker and DAPI after incubation with Te nanoneedles (scale bars, 10 μm). e) PA images at the tumor site before and after the injection of 1D Te nanoneedles (50 μL, 30 mg L^{-1}). f) Schematic of imaging-guided combined PTT + chemotherapy by using 1D Te-nanoneedle-based nanoplatform. g) Relative tumor volumes after various treatments on day 15 post-treatment. h) Photograph of tumors from various treated mice at day 15 post-treatment.

therapeutic effects in the future. From a chemical synthesis point of view, the nano-Se and nano-Te can be readily to nucleate and grow on the surfaces of anchors. Importantly, the most used 2D materials, such as graphene, GO, MXene and BP, with super-high specific surface areas (SSA) and excellent optical properties, may be ideal anchors to load nano-Se or nano-Te. As a result, Se- or Te-based nanohybrids with intriguing physical properties will be structured, which may have great potential in future cancer treatments.

Acknowledgements

This work was supported by the Science and Technology Innovation Commission of Shen Zhen (grant nos. JCYJ20170818091233245, KQTD20170810105439418), Natural Science Foundation of China (grant no. 81701819), the Natural Science Foundation of Guangdong Province (grant nos. 2019A1515010790 and 2017A030310495), the Scientific Research Starting Foundation for the Youth Scholars of Shenzhen University (grant no. 2019107). The authors thank Gillian Campbell, Ph.D., from Liwen Bianji, Edanz Group China, for editing the English text of a draft of this manuscript.

Conflict of Interest

The authors declare no conflict of interest.

Keywords

anticancer materials, nanomaterials, selenium, tellurium

Received: February 17, 2020
Revised: April 16, 2020
Published online: June 14, 2020

[1] H. Liu, Y. Du, Y. Deng, D. Y. Peide, *Chem. Soc. Rev.* **2015**, *44*, 2732.
[2] W. Lei, G. Liu, J. Zhang, M. Liu, *Chem. Soc. Rev.* **2017**, *46*, 3492.
[3] Z. He, Y. Yang, J.-W. Liu, S.-H. Yu, *Chem. Soc. Rev.* **2017**, *46*, 2732.
[4] R. Gui, H. Jin, Z. Wang, J. Li, *Chem. Soc. Rev.* **2018**, *47*, 6795.
[5] S. M. Beladi-Mousavi, M. Pumera, *Chem. Soc. Rev.* **2018**, *47*, 6964.
[6] M. Qiu, W. X. Ren, T. Jeong, M. Won, G. Y. Park, D. K. Sang, L.-P. Liu, H. Zhang, J. S. Kim, *Chem. Soc. Rev.* **2018**, *47*, 5588.
[7] W. Tao, N. Kong, X. Ji, Y. Zhang, A. Sharma, J. Ouyang, B. Qi, J. Wang, N. Xie, C. Kang, *Chem. Soc. Rev.* **2019**, *48*, 2891.
[8] S. Zhang, S. Guo, Z. Chen, Y. Wang, H. Gao, J. Gómez-Herrero, P. Ares, F. Zamora, Z. Zhu, H. Zeng, *Chem. Soc. Rev.* **2018**, *47*, 982.
[9] M. Pumera, Z. Sofer, *Adv. Mater.* **2017**, *29*, 1605299.
[10] D. Mao, S. Zhang, Y. Wang, X. Gan, W. Zhang, T. Mei, Y. Wang, Y. Wang, H. Zeng, J. Zhao, *Opt. Express* **2015**, *23*, 27509.
[11] P. Guo, J. Xu, K. Gong, X. Shen, Y. Lu, Y. Qiu, J. Xu, Z. Zou, C. Wang, H. Yan, Y. Luo, A. Pan, H. Zhang, J. C. Ho, K. M. Yu, *ACS Nano* **2016**, *10*, 8474.
[12] P. Wan, X. Wen, C. Sun, B. K. Chandran, H. Zhang, X. Sun, X. Chen, *Small* **2015**, *11*, 5409.
[13] S. Bai, C. Sun, H. Yan, X. Sun, H. Zhang, L. Luo, X. Lei, P. Wan, X. Chen, *Small* **2015**, *11*, 5807.
[14] Q. Bao, H. Zhang, C. Pan, *Comput. Mater. Sci.* **2007**, *39*, 616.
[15] Q. Bao, H. Zhang, C. Pan, *Appl. Phys. Lett.* **2006**, *89*, 063124.
[16] Z. Liu, J. T. Robinson, S. M. Tabakman, K. Yang, H. Dai, *Mater. Today* **2011**, *14*, 316.
[17] X. Shi, H. Gong, Y. Li, C. Wang, L. Cheng, Z. Liu, *Biomaterials* **2013**, *34*, 4786.
[18] B. Tian, C. Wang, S. Zhang, L. Feng, Z. Liu, *ACS Nano* **2011**, *5*, 7000.
[19] K. Yang, J. Wan, S. Zhang, B. Tian, Y. Zhang, Z. Liu, *Biomaterials* **2012**, *33*, 2206.
[20] W. Zhang, Z. Guo, D. Huang, Z. Liu, X. Guo, H. Zhong, *Biomaterials* **2011**, *32*, 8555.
[21] J. T. Robinson, S. M. Tabakman, Y. Liang, H. Wang, H. Sanchez Casalongue, D. Vinh, H. Dai, *J. Am. Chem. Soc.* **2011**, *133*, 6825.
[22] Z. Huang, Z. Zhang, X. Qi, X. Ren, G. Xu, P. Wan, X. Sun, H. Zhang, *Nanoscale* **2016**, *8*, 13273.
[23] Z. Zhang, Y. Liu, L. Ren, H. Zhang, Z. Huang, X. Qi, X. Wei, J. Zhong, *Electrochim. Acta* **2016**, *200*, 142.
[24] H. Zhang, D. Tang, L. Zhao, Q. Bao, K. P. Loh, *Opt. Commun.* **2010**, *283*, 3334.
[25] Y. Song, H. Zhang, D. Tang, D. Shen, *Opt. Express* **2012**, *20*, 27283.
[26] Z. T. Wang, Y. Chen, C. J. Zhao, H. Zhang, S. C. Wen, *IEEE Photonics J.* **2012**, *4*, 869.
[27] G. Zheng, Y. Chen, H. Huang, C. Zhao, S. Lu, S. Chen, H. Zhang, S. Wen, *ACS Appl. Mater. Interfaces* **2013**, *5*, 10288.
[28] R. Zhou, P. Tang, Y. Chen, S. Chen, C. Zhao, H. Zhang, S. Wen, *Appl. Opt.* **2014**, *53*, 254.
[29] Y. Jiang, L. Miao, G. Jiang, Y. Chen, X. Qi, X. F. Jiang, H. Zhang, S. Wen, *Sci. Rep.* **2015**, *5*, 16372.
[30] H. Mu, Z. Wang, J. Yuan, S. Xiao, C. Chen, Y. Chen, Y. Chen, J. Song, Y. Wang, Y. Xue, H. Zhang, Q. Bao, *ACS Photonics* **2015**, *2*, 832.
[31] Y. F. Song, H. Zhang, L. M. Zhao, D. Y. Shen, D. Y. Tang, *Opt. Express* **2016**, *24*, 1814.
[32] J. Ge, M. Lan, B. Zhou, W. Liu, L. Guo, H. Wang, Q. Jia, G. Niu, X. Huang, H. Zhou, *Nat. Commun.* **2014**, *5*, 4596.
[33] Y. Du, S. Guo, *Nanoscale* **2016**, *8*, 2532.
[34] S. Zhu, Y. Song, J. Wang, H. Wan, Y. Zhang, Y. Ning, B. Yang, *Nano Today* **2017**, *13*, 10.
[35] C. Gutiérrez, L. Brown, C.-J. Kim, J. Park, A. N. Pasupathy, *Nat. Phys.* **2016**, *12*, 1069.
[36] K. Yang, L. Feng, Z. Liu, *Adv. Drug Delivery Rev.* **2016**, *105*, 228.
[37] Z. Gu, S. Zhu, L. Yan, F. Zhao, Y. Zhao, *Adv. Mater.* **2019**, *31*, 1800662.
[38] J. Liu, J. Dong, T. Zhang, Q. Peng, *J. Controlled Release* **2018**, *286*, 64.
[39] K. Yang, L. Feng, X. Shi, Z. Liu, *Chem. Soc. Rev.* **2013**, *42*, 530.
[40] L. V. Nair, S. S. Nazeer, R. S. Jayasree, A. Ajayaghosh, *ACS Nano* **2015**, *9*, 5825.
[41] A. K. Rengan, A. B. Bukhari, A. Pradhan, R. Malhotra, R. Banerjee, R. Srivastava, A. De, *Nano Lett.* **2015**, *15*, 842.
[42] C. Wang, J. Li, C. Amatore, Y. Chen, H. Jiang, X. M. Wang, *Angew. Chem., Int. Ed.* **2011**, *50*, 11644.
[43] W. Cai, T. Gao, H. Hong, J. Sun, *Nanotechnol. Sci. Appl.* **2008**, *1*, 17.
[44] S. Wang, K. J. Chen, T. H. Wu, H. Wang, W. Y. Lin, M. Ohashi, P. Y. Chiou, H. R. Tseng, *Angew. Chem., Int. Ed.* **2010**, *49*, 3777.
[45] S. Jain, D. Hirst, J. O'sullivan, *Br. J. Radiol.* **2012**, *85*, 101.
[46] G. Peng, U. Tisch, O. Adams, M. Hakim, N. Shehada, Y. Y. Broza, S. Billan, R. Abdah-Bortnyak, A. Kuten, H. Haick, *Nat. Nanotechnol.* **2009**, *4*, 669.
[47] R. Popovtzer, A. Agrawal, N. A. Kotov, A. Popovtzer, J. Balter, T. E. Carey, R. Kopelman, *Nano Lett.* **2008**, *8*, 4593.
[48] X. Huang, P. K. Jain, I. H. El-Sayed, M. A. El-Sayed, *Nanomedicine.* **2007**, *2*, 681.
[49] X. Huang, P. K. Jain, I. H. El-Sayed, M. A. El-Sayed, *Laser. Med. Sci.* **2008**, *23*, 217.
[50] I. H. El-Sayed, X. Huang, M. A. El-Sayed, *Nano Lett.* **2005**, *5*, 829.
[51] D. B. Chithrani, S. Jelveh, F. Jalali, M. van Prooijen, C. Allen, R. G. Bristow, R. P. Hill, D. A. Jaffray, *Radiat. Res.* **2010**, *173*, 719.
[52] J. Nam, N. Won, H. Jin, H. Chung, S. Kim, *J. Am. Chem. Soc.* **2009**, *131*, 13639.
[53] D. Pissuwan, S. M. Valenzuela, M. B. Cortie, *Trends Biotechnol.* **2006**, *24*, 62.
[54] I. H. El-Sayed, X. Huang, M. A. El-Sayed, *Cancer Lett.* **2006**, *239*, 129.
[55] B. Kang, M. A. Mackey, M. A. El-Sayed, *J. Am. Chem. Soc.* **2010**, *132*, 1517.
[56] X. Liang, X. Ye, C. Wang, C. Xing, Q. Miao, Z. Xie, X. Chen, X. Zhang, H. Zhang, L. Mei, *J. Controlled Release* **2019**, *296*, 150.
[57] M. Qiu, D. Wang, W. Liang, L. Liu, Y. Zhang, X. Chen, D. K. Sang, C. Xing, Z. Li, B. Dong, *Proc. Natl. Acad. Sci. USA* **2018**, *115*, 501.
[58] C. Xing, S. Chen, M. Qiu, X. Liang, Q. Liu, Q. Zou, Z. Li, Z. Xie, D. Wang, B. Dong, *Adv. Healthcare Mater.* **2018**, *7*, 1701510.
[59] C. Xing, G. Jing, X. Liang, M. Qiu, Z. Li, R. Cao, X. Li, D. Fan, H. Zhang, *Nanoscale* **2017**, *9*, 8096.
[60] J. Shao, H. Xie, H. Huang, Z. Li, Z. Sun, Y. Xu, Q. Xiao, X.-F. Yu, Y. Zhao, H. Zhang, *Nat. Commun.* **2016**, *7*, 12967.
[61] C. Sun, L. Wen, J. Zeng, Y. Wang, Q. Sun, L. Deng, C. Zhao, Z. Li, *Biomaterials* **2016**, *91*, 81.
[62] Z. Sun, Y. Zhao, Z. Li, H. Cui, Y. Zhou, W. Li, W. Tao, H. Zhang, H. Wang, P. K. Chu, *Small* **2017**, *13*, 1602896.
[63] W. Tao, X. Zhu, X. Yu, X. Zeng, Q. Xiao, X. Zhang, X. Ji, X. Wang, J. Shi, H. Zhang, *Adv. Mater.* **2017**, *29*, 1603276.
[64] C. Xing, L. Liu, D. Fan, Z. Peng, H. Zhang, *FlatChem* **2019**, *13*, 8.
[65] X. Zhang, H. Xie, Z. Liu, C. Tan, Z. Luo, H. Li, J. Lin, L. Sun, W. Chen, Z. Xu, *Angew. Chem., Int. Ed.* **2015**, *54*, 3653.
[66] X. Qian, Z. Gu, Y. Chen, *Mater. Horiz.* **2017**, *4*, 800.
[67] W. Chen, J. Ouyang, H. Liu, M. Chen, K. Zeng, J. Sheng, Z. Liu, Y. Han, L. Wang, J. Li, *Adv. Mater.* **2017**, *29*, 1603864.
[68] X. Chen, G. Xu, X. Ren, Z. Li, X. Qi, K. Huang, H. Zhang, Z. Huang, J. Zhong, *J. Mater. Chem. A* **2017**, *5*, 6581.
[69] M. Qiu, Z. T. Sun, D. K. Sang, X. G. Han, H. Zhang, C. M. Niu, *Nanoscale* **2017**, *9*, 13384.
[70] Y. Song, Z. Liang, X. Jiang, Y. Chen, Z. Li, L. Lu, Y. Ge, K. Wang, J. Zheng, S. Lu, J. Ji, H. Zhang, *2D Mater.* **2017**, *4*, 045010.

[71] X. Ren, Z. Li, Z. Huang, D. Sang, H. Qiao, X. Qi, J. Li, J. Zhong, H. Zhang, *Adv. Funct. Mater.* **2017**, *27*, 1606834.
[72] J. Ma, S. Lu, Z. Guo, X. Xu, H. Zhang, D. Tang, D. Fan, *Opt. Express* **2015**, *23*, 22643.
[73] Y. Song, S. Chen, Q. Zhang, L. Li, L. Zhao, H. Zhang, D. Tang, *Opt. Express* **2016**, *24*, 25933.
[74] Z. Wang, Y. Xu, S. C. Dhanabalan, J. Sophia, C. Zhao, C. Xu, Y. Xiang, J. Li, H. Zhang, *IEEE Photonics J.* **2016**, *8*, 1.
[75] J. Zheng, Z. Yang, C. Si, Z. Liang, X. Chen, R. Cao, Z. Guo, K. Wang, Y. Zhang, J. Ji, M. Zhang, D. Fan, H. Zhang, *ACS Photonics* **2017**, *4*, 1466.
[76] J. Du, M. Zhang, Z. Guo, J. Chen, X. Zhu, G. Hu, P. Peng, Z. Zheng, H. Zhang, *Sci. Rep.* **2017**, *7*, 42357.
[77] Y. Xu, X.-F. Jiang, Y. Ge, Z. Guo, Z. Zeng, Q.-H. Xu, H. Zhang, X.-F. Yu, D. Fan, *J. Mater. Chem. C* **2017**, *5*, 3007.
[78] Z. Chu, J. Liu, Z. Guo, H. Zhang, *Opt. Mater. Express* **2016**, *6*, 2374.
[79] J. Liu, J. Liu, Z. Guo, H. Zhang, W. Ma, J. Wang, L. Su, *Opt. Express* **2016**, *24*, 30289.
[80] J. Li, H. Luo, B. Zhai, R. Lu, Z. Guo, H. Zhang, Y. Liu, *Sci. Rep.* **2016**, *6*, 30361.
[81] M. Qiu, W. Ren, T. Jeong, M. Won, G. Park, D. Sang, L. Liu, H. Zhang, J. Kim, *Chem. Soc. Rev.* **2018**, *47*, 5588.
[82] F. Yin, K. Hu, S. Chen, D. Wang, J. Zhang, M. Xie, D. Yang, M. Qiu, H. Zhang, Z. g. Li, *J. Mater. Chem. B* **2017**, *5*, 5433.
[83] M. Qiu, D. Wang, W. Liang, L. Liu, Y. Zhang, X. Chen, D. K. Sang, C. Xing, Z. Li, B. Dong, F. Xing, D. Fan, S. Bao, H. Zhang, Y. Cao, *Proc. Natl. Acad. Sci. USA* **2018**, *115*, 501.
[84] Y. Zhao, H. Wang, H. Huang, Q. Xiao, Y. Xu, Z. Guo, H. Xie, J. Shao, Z. Sun, W. Han, *Angew. Chem., Int. Ed.* **2016**, *55*, 5003.
[85] Q. Zhou, Q. Chen, Y. Tong, J. Wang, *Angew. Chem., Int. Ed.* **2016**, *55*, 11437.
[86] H. U. Lee, S. Y. Park, S. C. Lee, S. Choi, S. Seo, H. Kim, J. Won, K. Choi, K. S. Kang, H. G. Park, *Small* **2016**, *12*, 214.
[87] W. Tao, X. Ji, X. Xu, M. A. Islam, Z. Li, S. Chen, P. E. Saw, H. Zhang, Z. Bharwani, Z. Guo, *Angew. Chem., Int. Ed.* **2017**, *56*, 11896.
[88] W. Tao, X. Ji, X. Zhu, L. Li, J. Wang, Y. Zhang, P. E. Saw, W. Li, N. Kong, M. A. Islam, *Adv. Mater.* **2018**, *30*, 1802061.
[89] P. Ares, J. J. Palacios, G. Abellán, J. Gómez-Herrero, F. Zamora, *Adv. Mater.* **2018**, *30*, 1703771.
[90] L. Miao, J. Yi, Q. Wang, D. Feng, H. He, S. Lu, C. Zhao, H. Zhang, S. Wen, *Opt. Mater. Express* **2016**, *6*, 2244.
[91] X. Jiang, S. Gross, H. Zhang, Z. Guo, M. J. Withford, A. Fuerbach, *Ann. Phys.* **2016**, *528*, 543.
[92] L. Lu, Z. Liang, L. Wu, Y. Chen, Y. Song, S. C. Dhanabalan, J. S. Ponraj, B. Dong, Y. Xiang, F. Xing, D. Fan, H. Zhang, *Laser Photonics Rev.* **2018**, *12*, 1870012.
[93] Q. Wang, Y. Chen, L. Miao, G. Jiang, S. Chen, J. Liu, X. Fu, C. Zhao, H. Zhang, *Opt. Express* **2015**, *23*, 7681.
[94] L. Meng, L. Ai-Ping, Z. Xu-Wu, Z. Nian, L. Hao, L. Zhi-Chao, X. Wen-Cheng, C. Yu, Z. Chu-Jun, Z. Han, *J. Lightwave Technol.* **2015**, *33*, 2056.
[95] Z. Wang, H. Mu, J. Yuan, C. Zhao, Q. Bao, H. Zhang, *IEEE J. Sel. Top. Quantum Electron.* **2017**, *23*, 195.
[96] S. Chen, L. Miao, X. Chen, Y. Chen, C. Zhao, S. Datta, Y. Li, Q. Bao, H. Zhang, Y. Liu, S. Wen, D. Fan, *Adv. Opt. Mater.* **2015**, *3*, 1769.
[97] Q. Wang, Y. Chen, G. Jiang, L. Miao, C. Zhao, X. Fu, S. Wen, H. Zhang, *IEEE Photonics J.* **2015**, *7*, 1.
[98] M. Liu, Z. R. Cai, S. Hu, A. P. Luo, C. J. Zhao, H. Zhang, W. C. Xu, Z. C. Luo, *Opt. Lett.* **2015**, *40*, 4767.
[99] Y. Tan, H. Zhang, C. Zhao, S. Akhmadaliev, S. Zhou, F. Chen, *Opt. Lett.* **2015**, *40*, 637.
[100] Y. Chen, M. Wu, P. Tang, S. Chen, J. Du, G. Jiang, Y. Li, C. Zhao, H. Zhang, S. Wen, *Laser Phys. Lett.* **2014**, *11*.
[101] C. Shuqing, W. Qingkai, Z. Chujun, L. Ying, Z. Han, W. Shuangchun, *J. Lightwave Technol.* **2014**, *32*, 4438.
[102] L. Lu, X. Tang, R. Cao, L. Wu, Z. Li, G. Jing, B. Dong, S. Lu, Y. Li, Y. Xiang, J. Li, D. Fan, H. Zhang, *Adv. Opt. Mater.* **2017**, *5*, 1700301.
[103] L. Gao, W. Huang, J. D. Zhang, T. Zhu, H. Zhang, C. J. Zhao, W. Zhang, H. Zhang, *Appl. Opt.* **2014**, *53*, 5117.
[104] W. Man, C. Yu, Z. Han, W. Shuangchun, *IEEE J. Quantum Electron.* **2014**, *50*, 393.
[105] C. Yu, Z. Chujun, C. Shuqing, D. Juan, T. Pinghua, J. Guobao, Z. Han, W. Shuangchun, T. Dingyuan, *IEEE J. Sel. Top. Quantum Electron.* **2014**, *20*, 315.
[106] Y. Peiguang, L. Rongyong, C. Hao, Z. Han, L. Aijiang, Y. Haipeng, R. Shuangchen, *IEEE Photonics Technol. Lett.* **2015**, *27*, 264.
[107] X. Jiang, S. Liu, W. Liang, S. Luo, Z. He, Y. Ge, H. Wang, R. Cao, F. Zhang, Q. Wen, J. Li, Q. Bao, D. Fan, H. Zhang, *Laser Photonics Rev.* **2018**, *12*, 1870013.
[108] B. Wang, H. Yu, H. Zhang, C. Zhao, S. Wen, H. Zhang, J. Wang, *IEEE Photonics J.* **2014**, *6*, 1.
[109] P. Li, G. Zhang, H. Zhang, C. Zhao, J. Chi, Z. Zhao, C. Yang, H. Hu, Y. Yao, *IEEE Photonics Technol. Lett.* **2014**, *26*, 1912.
[110] H. Xie, Z. Li, Z. Sun, J. Shao, X. F. Yu, Z. Guo, J. Wang, Q. Xiao, H. Wang, Q. Q. Wang, H. Zhang, P. K. Chu, *Small* **2016**, *12*, 4136.
[111] W. Tao, X. Ji, X. Xu, M. A. Islam, Z. Li, S. Chen, P. E. Saw, H. Zhang, Z. Bharwani, Z. Guo, J. Shi, O. C. Farokhzad, *Angew. Chem., Int. Ed.* **2017**, *56*, 11896.
[112] S. Chaudhary, A. Umar, S. Mehta, *J. Biomed. Nanotechnol.* **2014**, *10*, 3004.
[113] S. A. Wadhwani, U. U. Shedbalkar, R. Singh, B. A. Chopade, *Appl. Microbiol. Biotechnol.* **2016**, *100*, 2555.
[114] S. Chaudhary, A. Umar, S. Mehta, *Prog. Mater. Sci.* **2016**, *83*, 270.
[115] T. M. Sakr, M. Korany, K. V. Katti, *J. Drug Delivery Sci. Technol.* **2018**, *46*, 223.
[116] Q. Cui, J. Q. Wang, Y. G. Assaraf, L. Ren, P. Gupta, L. Wei, C. R. Ashby Jr, D. H. Yang, Z. S. Chen, *Drug Resist. Updates* **2018**, *41*, 1.
[117] A. Khurana, S. Tekula, M. A. Saifi, P. Venkatesh, C. Godugu, *Biomed. Pharmacother.* **2019**, *111*, 802.
[118] H. Vahidi, H. Barabadi, M. Saravanan, *J. Cluster Sci.* **2019**, *31*, 301.
[119] H. Tan, H. Y. Mo, A. Lau, Y. M. Xu, *Int. J. Mol. Sci.* **2019**, *20*, 75.
[120] A. Ghorbani, B. Omidvar, A. Parsi, *J. Nephropathol.* **2013**, *2*, 129.
[121] X. Qin, Z. Guo, Z. Liu, W. Zhang, M. Wan, B. Yang, *J. Photochem. Photobiol., B* **2013**, *120*, 156.
[122] G. Gonçalves, M. Vila, M. T. Portolés, M. Vallet-Regi, J. Gracio, P. A. A. Marques, *Adv. Healthcare Mater.* **2013**, *2*, 1072.
[123] Z. Liu, J. T. Robinson, X. Sun, H. Dai, *J. Am. Chem. Soc.* **2008**, *130*, 10876.
[124] L. Feng, L. Wu, X. Qu, *Adv. Mater.* **2013**, *25*, 168.
[125] H. Lin, Y. Wang, S. Gao, Y. Chen, J. Shi, *Adv. Mater.* **2018**, *30*, 1703284.
[126] H. Lin, X. Wang, L. Yu, Y. Chen, J. Shi, *Nano Lett.* **2017**, *17*, 384.
[127] Z. Liu, M. Zhao, H. Lin, C. Dai, C. Ren, S. Zhang, W. Peng, Y. Chen, *J. Mater. Chem. B* **2018**, *6*, 3541.
[128] C. Dai, H. Lin, G. Xu, Z. Liu, R. Wu, Y. Chen, *Chem. Mater.* **2017**, *29*, 8637.
[129] H. Lin, S. Gao, C. Dai, Y. Chen, J. Shi, *J. Am. Chem. Soc.* **2017**, *139*, 16235.
[130] C. Dai, Y. Chen, X. Jing, L. Xiang, D. Yang, H. Lin, Z. Liu, X. Han, R. Wu, *ACS Nano* **2017**, *11*, 12696.

[131] D. Zhang, Y. Cao, P. Li, J. Wu, X. Zong, *Sens. Actuators, B* **2018**, *265*, 529.
[132] C. Xing, S. Chen, X. Liang, Q. Liu, M. Qu, Q. Zou, J. Li, H. Tan, L. Liu, D. Fan, *ACS Appl. Mater. Interfaces* **2018**, *10*, 27631.
[133] C. Xing, D. Huang, S. Chen, Q. Huang, C. Zhou, Z. Peng, J. Li, X. Zhu, Y. Liu, Z. Liu, *Adv. Sci.* **2019**, *6*, 1900531.
[134] S. Zheng, X. Li, Y. Zhang, Q. Xie, Y.-S. Wong, W. Zheng, T. Chen, *Int. J. Nanomed.* **2012**, *7*, 3939.
[135] X. Liu, G. Deng, Y. Wang, Q. Wang, Z. Gao, Y. Sun, W. Zhang, J. Lu, J. Hu, *Nanoscale* **2016**, *8*, 8536.
[136] G. Wang, Y. Guo, G. Yang, L. Yang, X. Ma, K. Wang, L. Zhu, J. Sun, X. Wang, H. Zhang, *Sci. Rep.* **2016**, *6*, 31427.
[137] X. Gao, J. Zhang, L. Zhang, *Adv. Mater.* **2002**, *14*, 290.
[138] Y. Zhang, J. Wang, L. Zhang, *Langmuir* **2010**, *26*, 17617.
[139] W. Liu, X. Li, Y.-S. Wong, W. Zheng, Y. Zhang, W. Cao, T. Chen, *ACS Nano* **2012**, *6*, 6578.
[140] Y. Huang, L. He, W. Liu, C. Fan, W. Zheng, Y.-S. Wong, T. Chen, *Biomaterials* **2013**, *34*, 7106.
[141] B. Gates, Y. Yin, Y. Xia, *J. Am. Chem. Soc.* **2000**, *122*, 12582.
[142] J. Qin, G. Qiu, J. Jian, H. Zhou, L. Yang, A. Charnas, D. Y. Zemlyanov, C. Y. Xu, X. Xu, W. Wu, *ACS Nano* **2017**, *11*, 10222.
[143] C. Xing, Z. Xie, Z. Liang, W. Liang, T. Fan, J. S. Ponraj, S. C. Dhanabalan, D. Fan, H. Zhang, *Adv. Opt. Mater.* **2017**, *5*, 1700884.
[144] T. Yang, H. Ke, Q. Wang, Y. a. Tang, Y. Deng, H. Yang, X. Yang, P. Yang, D. Ling, C. Chen, *ACS Nano* **2017**, *11*, 10012.
[145] N. Yu, J. Li, Z. Wang, S. Yang, Z. Liu, Y. Wang, M. Zhu, D. Wang, Z. Chen, *Adv. Healthcare Mater.* **2018**, *7*, 1800643.
[146] Y. Lin, Y. Wu, R. Wang, G. Tao, P. F. Luo, X. Lin, G. Huang, J. Li, H. H. Yang, *Chem. Commun.* **2018**, *54*, 8579.
[147] J. Wen, K. Yang, X. Ding, H. Li, Y. Xu, F. Liu, S. Sun, *Inorg. Chem.* **2019**, *58*, 2987.
[148] W. Wu, G. Qiu, Y. Wang, R. Wang, P. Ye, *Chem. Soc. Rev.* **2018**, *47*, 7203.
[149] D. Zhang, D. Wang, P. Li, X. Zhou, X. Zong, G. Dong, *Sens. Actuators, B* **2018**, *255*, 1869.
[150] Q. Wang, M. Safdar, K. Xu, M. Mirza, Z. Wang, J. He, *ACS Nano* **2014**, *8*, 7497.
[151] Z. Xie, C. Xing, W. Huang, T. Fan, Z. Li, J. Zhao, Y. Xiang, Z. Guo, J. Li, Z. Yang, *Adv. Funct. Mater.* **2018**, *28*, 1705833.
[152] T. Chen, Y. S. Wong, W. Zheng, Y. Bai, L. Huang, *Colloids Surf., B* **2008**, *67*, 26.
[153] L. Tan, X. Jiang, Y. Zhang, H. Tang, S. Yao, Q. Xie, *Biosens. Bioelectron.* **2009**, *24*, 2268.
[154] J. S. Zheng, S. Y. Zheng, Y.-B. Zhang, B. Yu, W. Zheng, F. Yang, T. Chen, *Colloids Surf., B* **2011**, *83*, 183.
[155] Y. Li, X. Li, Y.-S. Wong, T. Chen, H. Zhang, C. Liu, W. Zheng, *Biomaterials* **2011**, *32*, 9068.
[156] H. Wu, X. Li, W. Liu, T. Chen, Y. Li, W. Zheng, C. W. Y. Man, M. K. Wong, K. H. Wong, *J. Mater. Chem.* **2012**, *22*, 9602.
[157] B. Yu, Y. Zhang, W. Zheng, C. Fan, T. Chen, *Inorg. Chem.* **2012**, *51*, 8956.
[158] F. Yang, Q. Tang, X. Zhong, Y. Bai, T. Chen, Y. Zhang, Y. Li, W. Zheng, *Int. J. Nanomed.* **2012**, *7*, 835.
[159] Y. Zhang, X. Li, Z. Huang, W. Zheng, C. Fan, T. Chen, *Nanomed.: Nanotechnol., Bio. Med.* **2013**, *9*, 74.
[160] J. Pi, H. Jin, R. Liu, B. Song, Q. Wu, L. Liu, J. Jiang, F. Yang, H. Cai, J. Cai, *Appl. Microbiol. Biotechnol.* **2013**, *97*, 1051.
[161] Y. Li, X. Li, W. Zheng, C. Fan, Y. Zhang, T. Chen, *J. Mater. Chem. B* **2013**, *1*, 6365.
[162] F. Gao, Q. Yuan, L. Gao, P. Cai, H. Zhu, R. Liu, Y. Wang, Y. Wei, G. Huang, J. Liang, *Biomaterials* **2014**, *35*, 8854.
[163] Y. Feng, J. Su, Z. Zhao, W. Zheng, H. Wu, Y. Zhang, T. Chen, *Dalton Trans.* **2014**, *43*, 1854.
[164] Q. Chen, Q. Yu, Y. Liu, D. Bhavsar, L. Yang, X. Ren, D. Sun, W. Zheng, J. Liu, L.-m. Chen, *Nanomed.: Nanotechnol., Bio. Med.* **2015**, *11*, 1773.
[165] W. Liao, Z. Yu, Z. Lin, Z. Lei, Z. Ning, J. M. Regenstein, J. Yang, J. Ren, *Sci. Rep.* **2016**, *5*, 18629.
[166] W. Zheng, C. Cao, Y. Liu, Q. Yu, C. Zheng, D. Sun, X. Ren, J. Liu, *Acta Biomater.* **2015**, *11*, 368.
[167] T. Liu, L. Zeng, W. Jiang, Y. Fu, W. Zheng, T. Chen, *Nanomed.: Nanotechnol., Bio. Med.* **2015**, *11*, 947.
[168] T. Nie, H. Wu, K. H. Wong, T. Chen, *J. Mater. Chem. B* **2016**, *4*, 2351.
[169] T. A. Mary, K. Shanthi, K. Vimala, K. Soundarapandian, *RSC Adv.* **2016**, *6*, 22936.
[170] Y. Li, Z. Lin, M. Zhao, T. Xu, C. Wang, H. Xia, H. Wang, B. Zhu, *Int. J Nanomed.* **2016**, *11*, 3065.
[171] Y. Chang, L. He, Z. Li, L. Zeng, Z. Song, P. Li, L. Chan, Y. You, X.-F. Yu, P. K. Chu, *ACS Nano* **2017**, *11*, 4848.
[172] M. Guo, Y. Li, Z. Lin, M. Zhao, M. Xiao, C. Wang, T. Xu, Y. Xia, B. Zhu, *RSC Adv.* **2017**, *7*, 52456.
[173] Q. Xie, W. Deng, X. Yuan, H. Wang, Z. Ma, B. Wu, X. Zhang, *Eur. J. Pharm. Biopharm.* **2018**, *122*, 87.
[174] X. Fang, X. Wu, C. e. Li, B. Zhou, X. Chen, T. Chen, F. Yang, *RSC Adv.* **2017**, *7*, 8178.
[175] L. Chan, L. He, B. Zhou, S. Guan, M. Bo, Y. Yang, Y. Liu, X. Liu, Y. Zhang, Q. Xie, *Chem. - Asian J.* **2017**, *12*, 3053.
[176] U. Luesakul, S. Puthong, N. Neamati, N. Muangsin, *Carbohydr. Polym.* **2018**, *181*, 841.
[177] X. Fang, C. e. Li, L. Zheng, F. Yang, T. Chen, *Chem. - Asian J.* **2018**, *13*, 996.
[178] X. Liu, Y. Wang, Q. Yu, G. Deng, Q. Wang, X. Ma, Q. Wang, J. Lu, *Colloids Surf., B* **2018**, *166*, 161.
[179] W. Huang, Y. Liang, C. Sang, C. Mei, X. Li, T. Chen, *J. Mater. Chem. B* **2018**, *6*, 3013.
[180] A. R. Shahverdi, F. Shahverdi, E. Faghfuri, F. Mavandadnejad, M. H. Yazdi, M. Amini, *Arch. Med. Res.* **2018**, *49*, 10.
[181] Y. Xia, M. Guo, T. Xu, Y. Li, C. Wang, Z. Lin, M. Zhao, B. Zhu, *Int. J. Nanomed.* **2018**, *13*, 1539.
[182] Y. Wang, X. Liu, G. Deng, J. Sun, H. Yuan, Q. Li, Q. Wang, J. Lu, *Nanoscale* **2018**, *10*, 2866.
[183] M. Chen, Y. Huang, X. Zhu, X. Hu, T. Chen, *Adv. Ther.* **2018**, *1*, 1800074.
[184] D. Cui, T. Liang, L. Sun, L. Meng, C. Yang, L. Wang, T. Liang, Q. Li, *Pharm. Biol.* **2018**, *56*, 528.
[185] T. Liu, C. Shi, L. Duan, Z. Zhang, L. Luo, S. Goel, W. Cai, T. Chen, *J. Mater. Chem. B* **2018**, *6*, 4756.
[186] S. Tang, T. Wang, M. Jiang, C. Huang, C. Lai, Y. Fan, Q. Yong, *Int. J. Biol. Macromol.* **2019**, *128*, 444.
[187] D. Cui, J. Ma, T. Liang, L. Sun, L. Meng, T. Liang, Q. Li, *Int. J. Biol. Macromol.* **2019**, *137*, 829.
[188] J. Huang, W. Huang, Z. Zhang, X. Lin, H. Lin, L. Peng, T. Chen, *ACS Appl. Mater. Interfaces* **2019**, *11*, 11177.
[189] D. Zeng, J. Zhao, K.-H. Luk, S.-T. Cheung, K.-H. Wong, T. Chen, *J. Agric. Food Chem.* **2019**, *67*, 2865.
[190] B. Yu, X. Li, W. Zheng, Y. Feng, Y.-S. Wong, T. Chen, *J. Mater. Chem. B* **2014**, *2*, 5409.
[191] H. Luo, F. Wang, Y. Bai, T. Chen, W. Zheng, *Colloids Surf., B* **2012**, *94*, 304.
[192] J. Pi, F. Yang, H. Jin, X. Huang, R. Liu, P. Yang, J. Cai, *Bioorg. Med. Chem. Lett.* **2013**, *23*, 6296.
[193] L. Zheng, C. e. Li, X. Huang, X. Lin, W. Lin, F. Yang, T. Chen, *Biomaterials* **2019**, *216*, 119220.
[194] Z. Ping, T. Liu, H. Xu, Y. Meng, W. Li, X. Xu, L. Zhang, *Nano Res.* **2017**, *10*, 3775.
[195] X. Chen, K. Cai, J. Fang, M. Lai, Y. Hou, J. Li, Z. Luo, Y. Hu, L. Tang, *Colloids Surf., B* **2013**, *103*, 149.

[196] V. S. Saji, T. Kumeria, K. Gulati, M. Prideaux, S. Rahman, M. Alsawat, A. Santos, G. J. Atkins, D. Losic, *J. Mater. Chem. B* **2015**, *3*, 7090.
[197] W. Huang, H. Wu, X. Li, T. Chen, *Chem. - Asian J.* **2016**, *11*, 2301.
[198] Y. Wu, T. Guo, Y. Qiu, Y. Lin, Y. Yao, W. Lian, L. Lin, J. Song, H. Yang, *Chem. Sci.* **2019**, *10*, 7068.
[199] W. Huang, Y. Huang, Y. You, T. Nie, T. Chen, *Adv. Funct. Mater.* **2017**, *27*, 1701388.
[200] X. Ji, N. Kong, J. Wang, W. Li, Y. Xiao, S. Gan, Y. Zhang, Y. Li, X. Song, Q. Xiong, S. Shi, Z. Li, W. Tao, H. Zhang, L. Mei, J. Shi, *Adv. Mater.* **2018**, *30*, 1803031.
[201] S. Chen, C. Xing, D. Huang, C. Zhou, B. Ding, Z. Peng, D. Wang, X. Zhu, S. Liu, Z. Cai, J. Wu, J. Zhao, Z. Wu, Y. Zhang, C. Wei, Q. Yan, H. Wang, D. Fan, L. Liu, H. Zhang, Y. Cao, *Sci. Adv.* **2020**, *6*, eaay6825.